THE TENSILE AND COMPRESSIVE PROPERTIES OF FOUR EXPERIMENTAL MAGNESIUM ALLOYS ASSESSED FOR LIGHT DUTY TRUCK OIL PANS

by

Mehmet Barış TANZER

B.S., Mechanical Engineering, Middle East Technical University, 2007

Submitted to the Institute for Graduate Studies in
Science and Engineering in partial fulfillment of
the requirements for the degree of
Master of Science

Graduate Program in Mechanical Engineering
Boğaziçi University

2009

ACKNOWLEDGEMENTS

I would like to express my gratitude to Assistant Professor Ercan Balıkçı for his invaluable guidance and help during the preparation of this thesis.

Also, I would like to thank to Hasan Sicim, Aidin Dario, Arün Altınçekiç, and Onur Yaman who are Mechanical Engineering graduate students; Bilge Gedik Uluocak from Advanced Technologies R&D Center at Boğaziçi University; Sabri Yıldırım from Yıldırım Döküm for supplying raw materials; Ercan Kurtuluş from Kurtuluş Makina for manufacturing of the necessary samples; Nuri Sönmez and Özgür Özdemir from Ford Otosan for supporting the thesis; my mother, my father, my sister, and all other members of my family for their patience and for giving me hope all year long. I thank them all.

ABSTRACT

THE TENSILE AND COMPRESSIVE PROPERTIES OF FOUR EXPERIMENTAL MAGNESIUM ALLOYS ASSESSED FOR LIGHT DUTY TRUCK OIL PANS

Light weight design has a great importance in the development process of new automobiles. In recent years, the oil prices have increased and the exhaust gases of ignition engines have become a bigger concern for global warming. Many new materials, especially magnesium alloys, have been developed and introduced into the automobile industry to decrease the weight of the vehicles and to increase fuel efficiency. For these significant reasons, using the best material available to optimize the fuel economy is very important.

In this thesis, four magnesium alloy compositions have been chosen, based on the AS21 and ACM522 magnesium alloys, suitable for light duty trucks oil pans. The experimental results of the microstructure, tensile strength, and compressive strength of the die cast alloys are presented for these compositions. In the metallographic analysis, Mg_2Si and β-$Mg_{17}Al_{12}$ intermetallic phases have been observed. The intermetallic compound Mg_2Si has appeared in two morphologies, polyhedral and the Chinese script. The β-$Mg_{17}Al_{12}$ intermetallic phase has been observed as blocky precipitates. The increase in the calcium content has been observed to increase the amount and thickness of the Mg_2Si Chinese script phases present within the alloy. This has been observed to increase the strength of the alloys. In addition, a CAE analysis has been performed for modal analysis. The optimum composition for the light duty trucks oil pans is selected according to the results of these experiments.

ÖZET

HAFİF TİCARİ ARAÇLARIN YAĞ KARTERLERİ İÇİN GELİŞTİRİLEN DÖRT DENEYSEL MAGNEZYUM ALAŞIMININ ÇEKME VE BASMA ÖZELLİKLERİ

Hafif tasarım, yeni otomobillerin geliştirilmesi sürecinde büyük önem taşımaktadır. Son yıllarda, petrol fiyatlarındaki ve motor egzoz gazlarındaki artış küresel ısınma için daha büyük bir tehlike yaratmaya başlamıştır. Birçok yeni malzeme, özellikle magnezyum alaşımlar, araçların ağırlıklarının azaltılması ve yakıt verimliliğinin arttırılması için geliştirilmiştir. Bu nedenlerden dolayı en uygun özellikleri olan malzemenin kullanımı yakıt verimliliğinin arttırılması için büyük önem taşımaktadır.

Bu tezde dört farklı magnezyum alaşım kompozisyonu, AS21 ve ACM522 alaşımı temel alınarak, hafif ticari araçların yağ karteri için deneysel olarak geliştirilmiştir. Bu dört farklı kompozisyon için numuneler kokil kalıpta dökülmüştür. Bu hazırlanan numunelerin mikro analiz, çekme, ve basma testleri sonuçlar sunulmuştur. Metalografik analizde Mg_2Si ve β-$Mg_{17}Al_{12}$ fazları görüntülendi. Mg_2Si fazı iki morfolojide görüntülendi, çokyüzlü ve Çin el yazısı şeklinde. β-$Mg_{17}Al_{12}$ fazı blok parçacıklar halinde görüldü. Kalsiyum miktarında ki artış Çin el yazısı şeklinde ki Mg_2Si fazının miktarını ve kalınlığını arttırdı. Bunun da alaşımların kuvvetini arttırdığı gözlemlendi. Daha sonra deneylerin sonucunda ulaşılan değerler, CAE analizinde kullanılarak magnezyum alaşımının yağ karteri şeklinde üretildiğinde ki doğal frekansları ve ivmelenmeleri incelenmiştir. Böylece araç üstünde ki kullanımının uygunluğu araştırılmıştır. Deneylerin sonunda, hafif ticari araçların yağ karterinde kullanılabilmesi için en uygun kompozisyon seçilmiştir.

TABLE OF CONTENTS

LIST OF FIGURES

LIST OF TABLES

LIST OF SYMBOLS / ABBREVATIONS

E	Young's Modulus
n	Strain hardening exponent
m	Strain-rate sensitivity
δ	Elongation
ε	Engineering Strain
ε_T	True Strain
ρ	Density
σ_y	Yield Strength
σ_{UTS}	Ultimate Tensile Strength
σ_F	Fracture Strength
σ	Engineering Stress
σ_t	True Stress
BSE	Back Scattered Electron
EDS	Energy Dispersive Spectroscopy
ESEM	Environmental Scanning Electron Microscope
FS	Fracture Strength
SEM	Scanning Electron Microscope
TEM	Transmission Electron Microscopy
UTS	Ultimate Tensile Strength
WDS	Wavelength Dispersive Spectroscopy
YS	Yield Strength

1. INTRODUCTION

In recent years, the world's resources and ecology have become increasingly important. A number of researches have been conducted in order to preserve these resources and protect the environment by controlling the human impact. As an example, European Union has a commitment to increase the fuel efficiency of vehicles by 35 per cent from the 1995 level until 2010 [1] and to reduce the CO_2 emissions from 156 g per km for average new cars to 70 g CO_2 per km by again 2010 [2].

One of the ways to reduce the emissions is producing lighter vehicles because lowering the weight of a vehicle will decrease the force to drive it, which will eventually reduce the fuel usage and emissions. Other ways to improve the fuel efficiency can be given as follows: using engines with higher efficiency such as diesel engines, optimizing the tire design, and decreasing the drag coefficient of vehicles in order to reduce the forces on a vehicle which are caused by wind. However, the most economical way to reduce the emissions is by reducing the weight of the cars, which is the reason for running extensive research programs conducted by several auto manufacturers to develop a light weight material [2].

Light-weight materials should posses certain properties such as strength, corrosion resistance, cost, creep resistance, and ease of producability. Many new light materials have been developed and introduced into the production stage. Among these, magnesium alloys appear to be the best materials choice because they mostly possess the above mentioned property criteria.

In today's automotive industry, most of the automotive parts are currently produced from steel and aluminum which are denser than magnesium alloys. By using a light magnesium alloy, therefore, the weight of the vehicles can be greatly reduced.

1.1. Magnesium and its Alloys

1.1.1. History

Magnesium is a well known material with a history of hundreds of years. The name of magnesium comes from an ancient Greek city named “Magnesia” in Greece. Although magnesium has been known for hundreds of years, the usage of magnesium started only two centuries ago. Three major steps as reported in [3] are as follows. The biggest step in the usage of magnesium came in 1808 when Sir Humphry Davy found magnesium oxide. After the production of magnesium oxide, Antoine Bussy produced pure magnesium metal in 1828. 58 years later, in 1886, the first commercial production of magnesium began in Germany.

After the first commercial production began, the usage of magnesium has rapidly increased. By the beginning of 1900s, magnesium production had rose to 10 tons per year and increased steadily till the First World War [4]. Magnesium alloys were started to be used in great amounts when these alloys were introduced into B-36 strategic bomber aircraft engines in 1930’s [5]. In World War II, magnesium production increased to its highest value of 232,000 tons per year in 1943 in Germany [6]. In the same years in the United States, first magnesium truck bodies were produced [5]. After World War II, Volkswagen used die cast magnesium alloys in crankcases and manual transmission cases in 19 million Beetles till 1980 and used about 380,000 tons of magnesium [7]. By using magnesium alloys in place of cast iron, Volkswagen reduced the weight of its automobiles by 50 kg. This was one of the largest magnesium alloy usage in automotive applications in the history of the industry. This usage was discontinued in the early 1980’s due to magnesium’s price instability and low creep resistance [8].

By 1990’s, the growth rate of the magnesium alloy usage had reached 15 per cent per year [9]. After 1990’s, the highest amount (5 million kg) of magnesium alloy usage was by Ford Motor Company, which used die-cast AM50 magnesium alloy as the key material in its front-end support assemblies for light-duty trucks [10]. Till 2025, it’s projected to keep this growth, and future predictions show at least a 100 kg magnesium usage per vehicle [11].

1.1.2. Metallurgical Production

In today's world, magnesium is a material which can be easily found. Magnesium is found in large deposits in earth's crust; it's the seventh abundant element [12]. It's found in large deposits of magnesite, dolomite, and other minerals. Also, it can be extracted from sea water, which provides an easy way to reach an unlimited source of this metal. Because of these reasons, commercial products of magnesium alloys are being produced in high volumes.

Till 1973, magnesium had been mostly produced from magnesite, which is mostly found in Austria and Greece. After 1973, the production of magnesium has been shifted towards seawater. Although sea water has only 0,5 weight per cent of magnesium, considering the amount of seawater, which is $1{,}44 \times 10^{18}$ tons on earth, there is $7{,}2 \times 10^{15}$ tons of magnesium, which is an unlimited source [13]. Using these sources many countries are producing magnesium. The amount of magnesium production in the world is given in Table 1.1. As can be seen from the statistics, China has doubled its production in past 5 years and become the major player in the magnesium market. Russia, Canada, USA, and Israel are the other suppliers in moderate amounts.

Table 1.1. Magnesium production throughout the world [14]

	2000	**2001**	**2002**	**2003**	**2004**	**2005**	**2006**
USA	74	43	35	43	43	43	43
Brasil	9	9	7	6	11	6	6
Canada	55	6	86	50	55	54	50
China	218	195	232	354	450	470	526
France	17	7	0	0	0	0	0
Israel	2	30	34	30	33	28	28
Russia	40	50	52	45	45	45	50

Magnesium is produced within these countries generally by two techniques: electrolysis and thermal reduction. The first technique, electrolysis of magnesium, uses two processes to produce magnesium from its ores: the Dow and Magnola processes. The

second technique, thermal reduction of magnesium, utilizes thermal reduction of magnesium oxide (MgO) by ferrosilicon, which is provided from carbonate ores [4]. Two processes are used for this technique: the Pidgeon and the Magnetherm processes. The latter method, the Magnetherm process, is basically used because of the low cost of the process and the availability of the materials used within this process thus is more widespread than the Pidgeon process.

The Dow process is the electrolysis of fused anhydrous magnesium chloride ($MgCl_2$) derived from magnesite, brine or seawater, which provides 80 per cent of magnesium used in today's industry. Most of the magnesium producing companies uses the Dow process for producing magnesium. The approach of the Magnola process, on the other hand, is the electrolysis of fused anhydrous $MgCl_2$ derived from serpentine ores. Thus, the Dow and the Magnola processes are similar processes. The difference between these processes is mainly based on the production of anhydrous $MgCl_2$. In the Dow process, sea water is first mixed with magnesium hydroxide and calcium oxide. Then magnesium hydroxide is neutralized and reduced to magnesium chloride solution. After this process, a fraction of water is removed in a dryer. In the last step of this process, the remaining water is removed by flashing off the water particles by adding small quantities of the partially dehydrated chloride into the mixture of magnesium, sodium, and calcium chlorides contained in the electrolytic cell. The process steps are given in Figure 1.1.

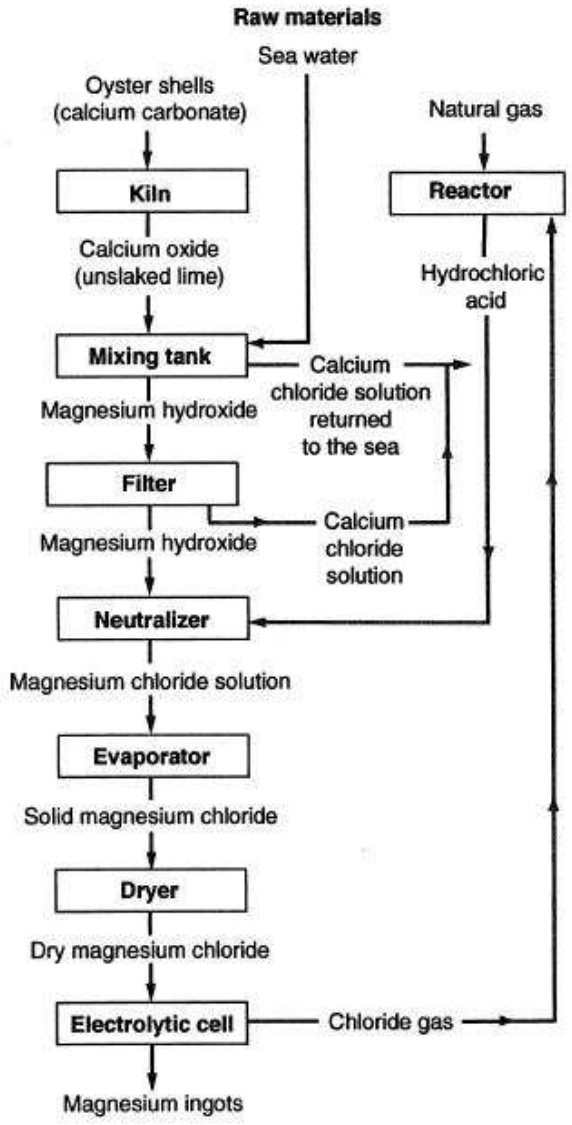

Figure 1.1. The Dow process [4]

In the Magnola electrolysis process, serpentine ores are used to produce magnesium chloride. Magnesium silicate contained in the tailings are leached with a strong hydrochloric acid to produce $MgCl_2$ solution, which is then purified by pH adjustment and ion exchange techniques to generate a concentrated ultra-high-purity brine for dehydration and electrolysis [4]. In the end with an electrolysis cell, magnesium ingots are produced. The process steps are given in Figure 1.2.

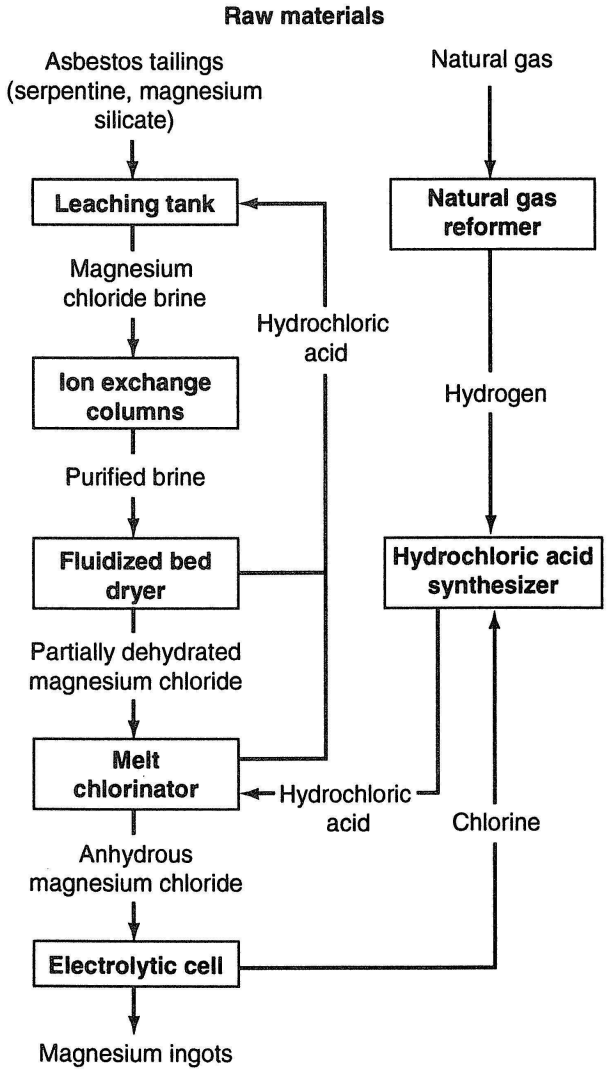

Figure 1.2. The Magnola process [4]

The thermal reduction processes differ through their production methods. The Pidgeon process is a thermic-reaction process, which uses externally heated retorts of relatively small diameter, each producing 120 kg of magnesium per day [4]. Firstly, magnesium carbonate and calcium carbonate are mixed with kiln in order to produce magnesium oxide and calcium oxide. Using a pulverizer calcined dolomite power is obtained. After this process, calcined dolomite powder and ferro-silicon powder is used in order to produce calcined dolomite and ferrosilicon powder mixture. Then, by a briquetting machine, calcined dolomite and ferrosilicon pellets are obtained. In the last steps of this process, retort furnaces and melting pots are used for obtaining magnesium ingots. The process steps are given in Figure 1.3.

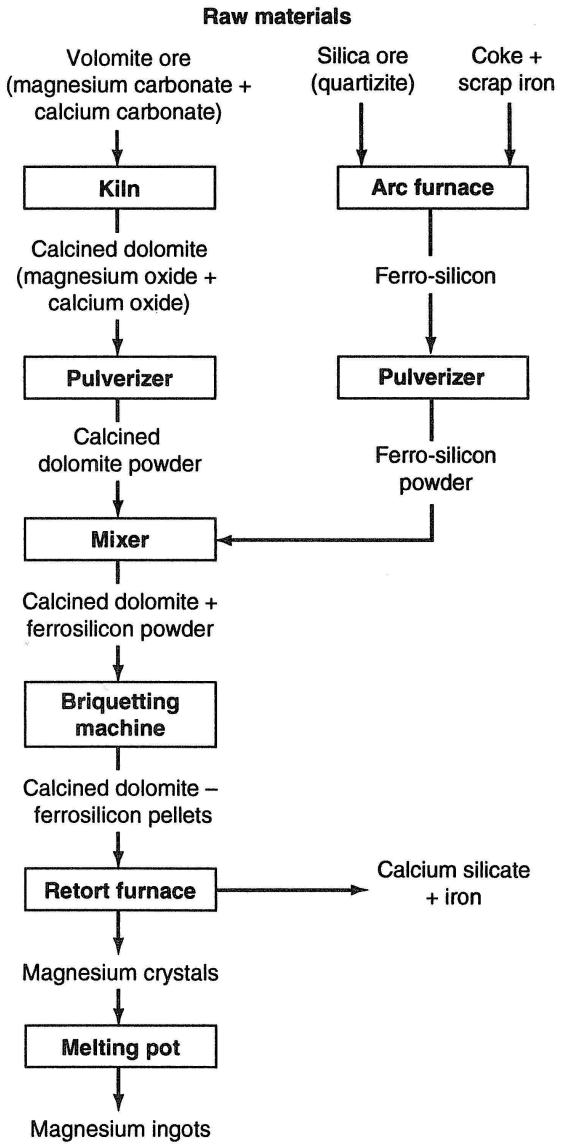

Figure 1.3. The Pidgeon process [4]

The Magnetherm process, which is a thermal reduction process, was developed just after the Second World War, and differs from the Pidgeon process in that magnesium is produced by a molten slag, which can be tagged off without breaking the vacuum. The process steps are given in Figure 1.4.

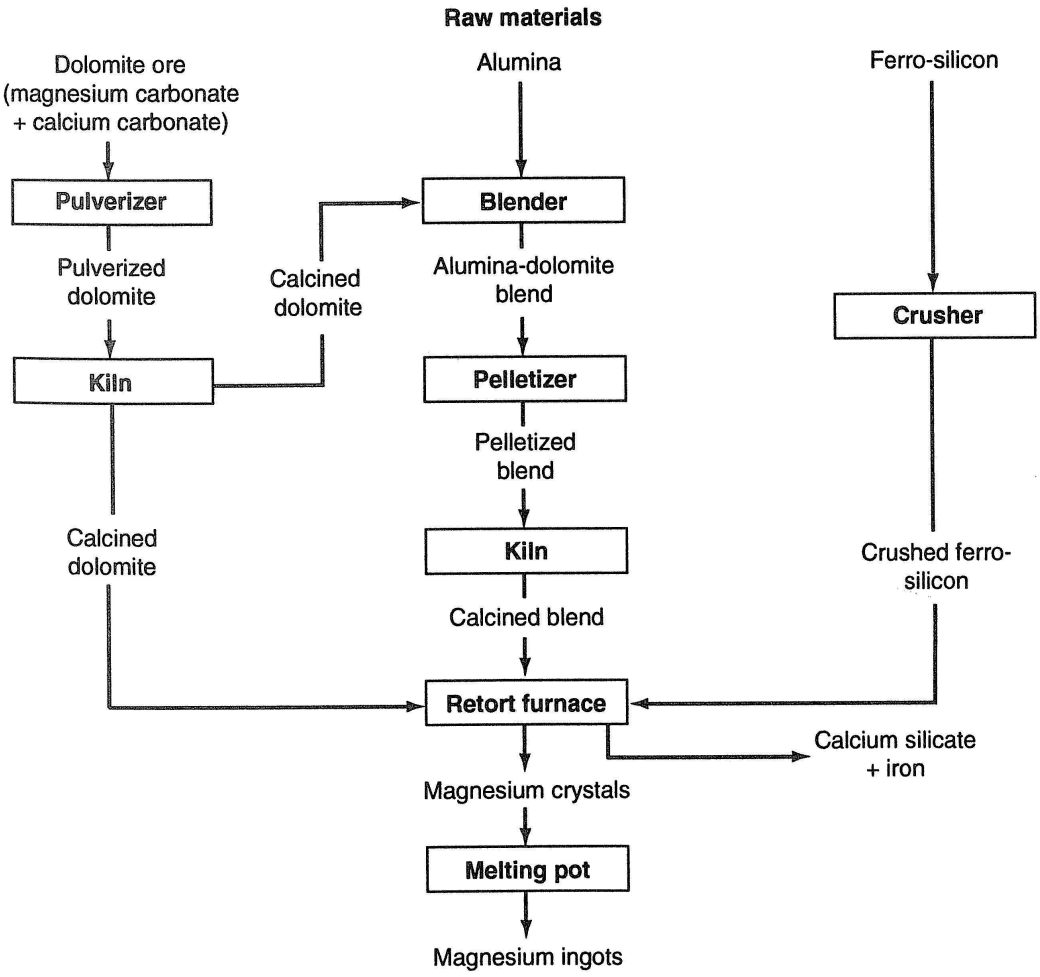

Figure 1.4. The Magnetherm process [4]

1.1.3. Relevant Phase Diagrams

The composition of the magnesium alloys that will be developed within this thesis will contain the elements Mg, Al, Si, and Ca. Hence, it is appropriate to investigate the binary phase diagrams of these elements.

1.1.3.1. Al-Ca phase diagram. The addition of aluminum and calcium into magnesium alloys increases the mechanical properties. The increase in the mechanical properties by secondary phase formation is obtained by the development of the Al_4Ca and Al_2Ca phases. The binary phase diagram of Al-Ca is given in Figure 1.5.

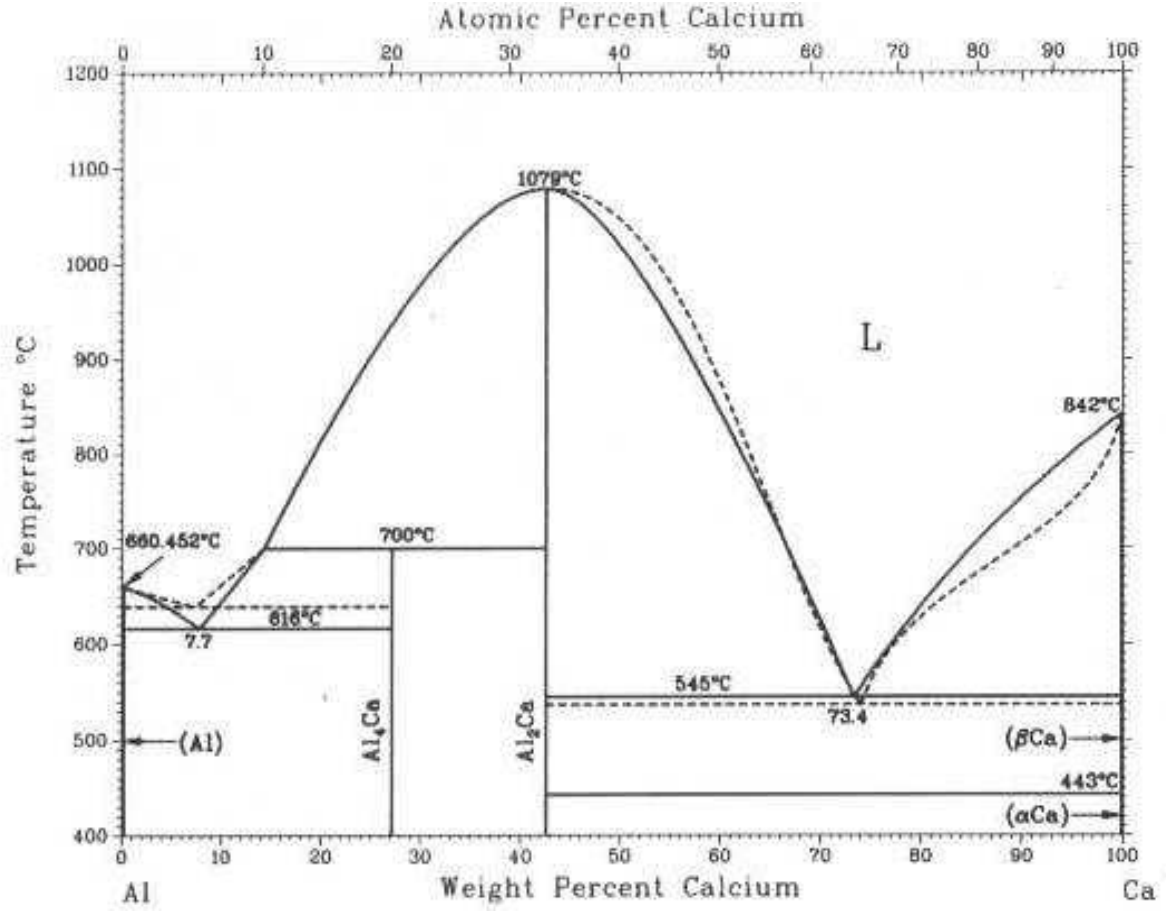

Figure 1.5. Al-Ca phase diagram (dashed lines: calculated) [15]

1.1.3.2. Mg-Ca Phase Diagram. Calcium addition into magnesium alloys significantly increases the creep resistance of the magnesium alloy by the formation of Mg_2Ca phase. The binary phase diagram of Mg-Ca is given in Figure 1.6.

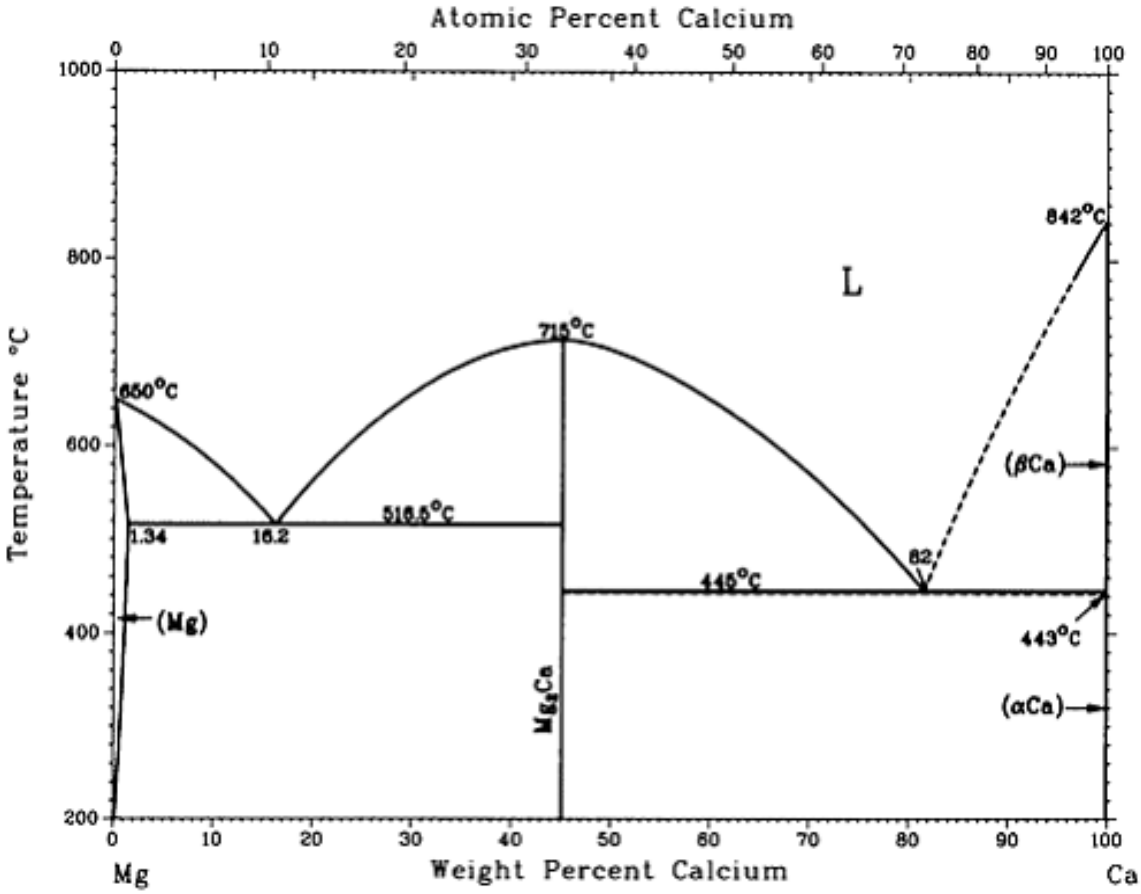

Figure 1.6. Mg-Ca phase diagram (dashed lines: calculated) [15]

1.1.3.3. Al-Mg phase diagram. Aluminum effectively increases the strength of the magnesium alloys. This increase can be obtained by the formation of the Al_3Mg_2 and $Al_{12}Mg_{17}$ phases. The binary phase diagram of Al-Mg is given in Figure 1.7.

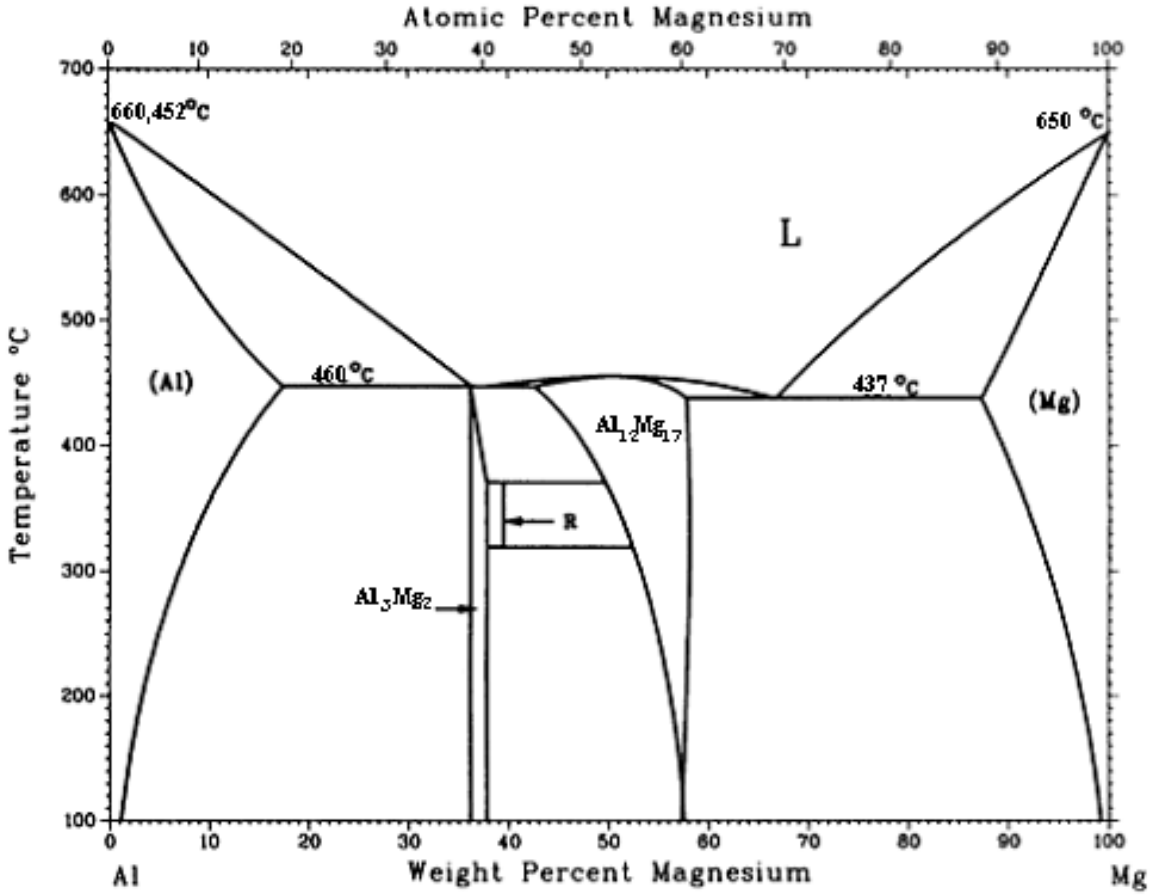

Figure 1.7. Al-Mg Phase diagram [15]

1.1.3.4. Mg-Si phase diagram**.** Silicon is an effective element which increases the creep resistance and castability of the magnesium alloys. These improvements in the properties of the alloys basically come from the Mg_2Si phases which are formed within the alloy. The binary phase diagram of the Mg-Si is given in Figure 1.8.

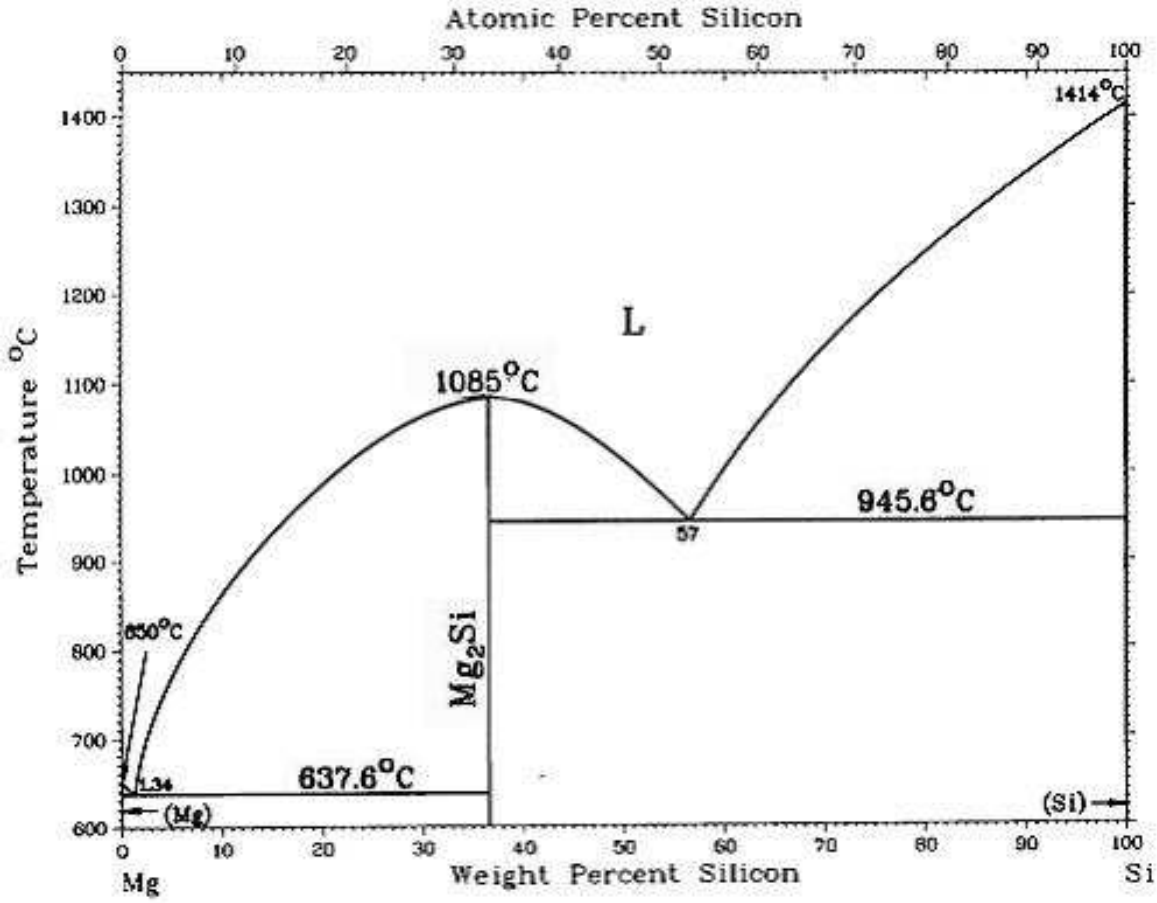

Figure 1.8. Mg-Si Phase diagram [15]

1.1.3.5. Al-Si phase diagram. Although, silicon and aluminum do not form any intermetallic phase they may form microconstituents with eutectic composition as can be seen in the binary phase diagram of Al-Si given in Figure 1.9.

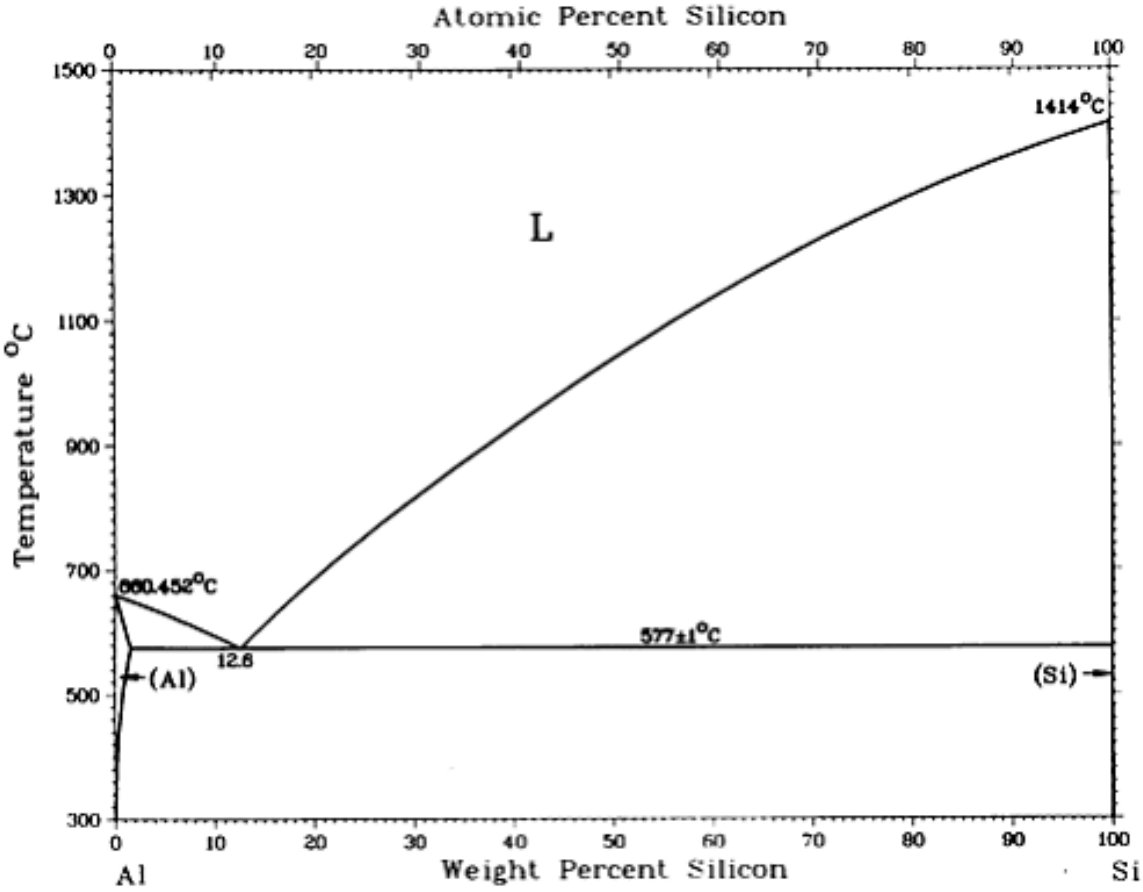

Figure 1.9. Al-Si Phase diagram [15]

1.1.4. Microstructures

Mechanical properties of materials depend strongly upon their microstructures. These properties can be improved by several means such as solid-solution hardening, reducing the grain size, and forming desired phases in the material.

In solid solution hardening, atoms of one or more elements are added to another, resulting in either substitutional or interstitial point defects in the crystal. These defects distort the crystal lattice, which act as barriers to dislocation propagation and thereby increasing the strength of the material.

In metals, grain size has a great effect on the mechanical properties of the alloys. Adjacent grains in a polycrystalline material have normally different orientations with a

common grain boundary. As a dislocation passes from one grain to another, since the grains have different orientations, a dislocation is required to change its orientation. This requires energy. As the grain boundary misorientation increases, the resistance against dislocation motion increases, which improves the strength of the material. Also, as small grained materials have a greater total grain boundary area, fine-grained materials have higher strength resulting from more blockages to dislocation motion.

The strength of materials can also be increased by forming secondary phases. These phases can be in a variety of sizes and are scattered uniformly within the original phase matrix. The mechanical properties are influenced by the characteristics of these particles. These particles increase the hardness and the strength of the material by acting as barriers to dislocation motion.

Accordingly, improved mechanical properties for alloys can be obtained by forming desired phases. Within this study, the phases to be formed by mixing Mg, Al, Ca, and Si will be discussed in this section. Assuming casting conditions produce similar grain sizes and alloying elements resulting in similar solid solution hardening, influence of the secondary phases will be more prevalent.

The given phase diagrams (see Figures 1.5-1.7) show that in a Mg-Ca-Al system, the phases that may be present in an alloy are Mg_2Ca (C14, hexagonal), Al_2Ca (C15, cubic), $(Mg, Al)_2Ca$ (C36, dihexagonal), Al_4Ca (DI_3, tetragonal), Al_3Mg_2 (hexagonal), and β-$Mg_{17}Al_{12}$ (A12, cubic) [16]. Each of these intermetallic phases influences the properties of the magnesium alloy differently. C15 phase is a stable phase which increases creep resistance [17]. The C36 phase has a more stable structure than C14 phase. Thus, the C36 phase better strengthens the grain boundaries and increases the creep resistance and strength of the alloy. β-$Mg_{17}Al_{12}$ phase is an unstable phase which decreases the creep resistance of the alloy, thus should be avoided [16]. Also, a study has reported that both Mg_2Ca and Al_2Ca phase form in as-cast Mg alloys when the Ca/Al mass ratio is more than 0.8 and that only the Al_2Ca phase develops when Ca/Al is less than 0.8 [18].

With the addition of silicon, it can be seen from the phase diagram that Mg_2Si phase forms in the microstructure of the alloy. This phase is finely dispersed when the material is

cast. This is a favorable phase because it significantly increases the creep resistance of the alloy [13].

1.1.5. Selected properties of magnesium alloys

Magnesium alloys, used in automotive industry, combine the optimal mechanical strength and stiffness; these alloys are the lightest structural metals in the industry [6]. Magnesium (ρ=1,738 g cm^{-3}) is 70 per cent lighter than steel (ρ=7,85 g cm^{-3}) and 35 per cent lighter than aluminum (ρ=2,7 g cm^{-3}). Therefore, a lighter vehicle can be obtained and up to 3 to 4 liters fuel reduction in 100 km can be achieved for the fuel efficiency in automotives using magnesium cast parts [2]. Still, magnesium alloys have advantages and disadvantages.

Advantages of magnesium alloys are their low density, optimal strength, stiffness, and good castability. The disadvantages are limited high-temperature strength, limited corrosion characteristics, and high cost. The main properties of magnesium base element for Mg alloys are shown in Table 1.2

Table 1.2. Physical properties of magnesium [19]

Physical Properties	
Density	1.74 g/cm^3
Crystal Structure	Hexagonal Close Packed
Mechanical Properties	
Hardness, Brinell	30.0
Tensile Strength, Ultimate	90.0 MPa
Tensile Strength, Yield	21.0 MPa
Elongation at Break	2.00 - 6.00 per cent
Modulus of Elasticity	44.0 GPa
Compressive Yield Strength	21.0 MPa
Thermal Properties	
Specific Heat Capacity	1.025 J/g-°C
Thermal Conductivity	159 W/m-K
Melting Point	648.3 - 649.3 °C

1.1.5.1. Effects of alloying elements. A worldwide research is conducted for new magnesium alloys and a high number of alloys have been developed for automotive usage [4]. In order to meet the requirements of the automotive parts, various alloying elements have been used to improve the properties of the alloys. Alloying elements are used in order to increase the creep resistance, ductility, castability, strength, stiffness, and corrosion resistance.

As each of the alloying elements has different effects in magnesium alloys, when constructing new magnesium alloys, the effect of these elements should be predicted beforehand in order to impart the required properties in the alloys. In the automotive industry, vigorous research efforts are put forward in order to investigate the effect of these elements. The effect of some of the alloying elements is given in Table 1.3.

Table 1.3. Roles of alloying elements in magnesium [4, 20 - 22]

Alloying Element	**Role in the Alloy**
Aluminum (Al)	Increases casting properties, strength, creep resistance, and corrosion resistance
Calcium (Ca)	Increases creep resistance, strength, decreases the grain size of the alloys, and prevents oxidation of the melt
Iron (Fe)	Increases grain refinement ability of alloys
Silicon (Si)	Significant increase of creep resistance and castability
Strontium (Sr)	Significant increase in elongation and higher yield strength
Thorium (Th)	Increases high temperature creep resistance and strength
Zinc (Zn)	Increases the fluidity of the molten magnesium alloy
Zirconium (Zr)	Increases the strength of the material
Rare Earth Elements (RE)	Increases the creep resistance and strength of the material
Manganese (Mn)	Increases the corrosion resistance and the yield strength

1.1.5.2. Commercially available magnesium alloys. Magnesium alloy notation generally starts with two capital letters followed by two or three numbers (i.e; AZ91D). The first two letters indicate the main alloying elements in the alloy. The first letter shows the alloying element with the highest concentration in the alloy and the second letter shows the alloying element with the second highest concentration in the alloy. The first number following the letters show the concentration of the first alloying element, and the second number shows the concentration of the second alloying element. The last letters following the numbers show the modifications in the alloy.

Table 1.4. Magnesium alloys

Alloy Acronym	**Elements in Alloy**
ACM	Mg, Al, Ca, and RE
ACX	Mg, Al, Ca, and Sr
AE	Mg, Al, and RE
AJ	Mg, Al, and Sr
AM	Mg, Al, and Mn
AS	Mg, Al, and Si
AZ	Mg, Al, and Zr
EQ	Mg, RE, Ag, and Cu
MRI	Mg, Al, Mn, Zn, Si, Cu, and Fe
QE	Mg, Ag, and Re
WE	Mg, Y, and Re
ZAC	Mg, Al, Cn, Ca, Sr, Fe, Ni, and Cu
ZC	Mg, Zi, and Cu
ZK	Mg, Zi, and Zr

Various magnesium alloy compositions have been developed already and efforts continue to discover a new alloying element to improve Mg alloy properties further. The alloys which are used in the automotive industry are given in Table 1.4. Most of these alloys have been innovated through conducting experiments on already existing alloys. A brief description of the characteristics of these alloys is as follows:

- **ACM** series is a group of one of the leading alloys used in mass production by Honda [23]. The alloys have high creep, thermal, corrosion resistance, strength, and recyclability. They are a competitive choice for oil pans. The alloys can be manufactured by High-Pressure-Die-Casting (HPDC) method.
- **ACX** series alloys are also manufactured by HPDC. They have creep resistance 25 per cent higher than AE42, cost and corrosion resistance equivalent to AZ91D alloys [24].
- **AE** series alloys have good strength and creep resistance and can be manufactured by HPDC [4].
- **AJ** series alloys have good creep resistance, high ductility (AJ62LX), and good die castability. These alloys have been innovated in Noranda Aluminum, Inc., North America and are recommended for usage in oil pans, transmission cases, and engine blocks [25]. The alloy can be manufactured by HPDC.
- **AM** series alloys have relatively high ductility, energy absorption, good strength, and castability. These series is recommended for usage in the interior applications for automotives [25].
- **AS** series is innovated in Norsk Hydro ASA, Norway. They have good strength and castability with good creep resistance up to 150^{o} C [26].
- **AZ** series alloys have reasonable cost, castability, good strength, and corrosion resistance. They are recommended for interior applications for automotives [27].
- **EQ** series is mainly used for short-time elevated-temperature application [4].
- **MRI** series is innovated by Dead Sea Magnesium Corporation. This series has low cost, good creep resistance, and ability to be employed at elevated temperature usage under high loads. These alloys are mainly used for automotive parts for service conditions up to 150^{o} C [28].
- **QE** series has good castability, yield strength, and creep resistance [4].
- **WE** series is used mainly in the applications of high strength and high temperatures [4].
- **ZAC** series, which is investigated for thixomolding, has good castability and strength [29].
- **ZC** series is relatively cheap and possesses good strength and ductility [4].
- **ZK** series has medium strength and good weldability [4].

1.1.5.3. Tensile and Compression Behavior. Magnesium alloys have a wide range of tensile and compression strength. If compared with compatible structural metals, magnesium alloys have similar tensile yield strength to density ratios (e.g.; the ratio is 114 for aluminum alloys and 117 for magnesium alloys). These properties depend on the microstructure of the alloys. In order to increase the tensile and compressive yield strength of the alloys, the resistance to dislocation motion within the microstructure of an alloy should be increased. Within this thesis, intermetallic phases will be formed in several new experimental magnesium alloys with increased mechanical properties using permanent-mold casting production technique.

The tension and compression tests provide quick and reliable mechanical property data for materials. A typical tensile test plot is given in Figure 1.10. In tension tests, the first linear part of the stress-strain graph provides data for the elastic properties of materials. Deformation in this region is called the elastic deformation and no permanent deformation develops in the material. It is the result of only the stretching of interatomic bonds and hence small changes in the interatomic spacings. The slope of the linear segment in the elastic region gives the Young's modulus or Elastic modulus, so the Young's modulus can be defined as the resistance of the bonds of adjacent atoms to separation. In order to prevent any permanent deformation within parts, they must be designed to have only elastic deformation. Yield strength is defined as the point, up to which only elastic deformation will occur.

After the elastic region of the material, the plastic region starts. The plot in this region increases till the Ultimate Tensile Strength (UTS) point on the graph. Till this point the cross-section of the material decreases uniformly, and strain hardening occurs. This results in increased number of dislocation within the structure which increases the strength. Just after this point, necking starts, which is a localized deformation in the material, and the material's strength starts to decrease till fracture so the plot decreases. The plastic deformation is the permanent deformation of the material in which the bonds of the atoms break and rebind with other new neighboring atoms.

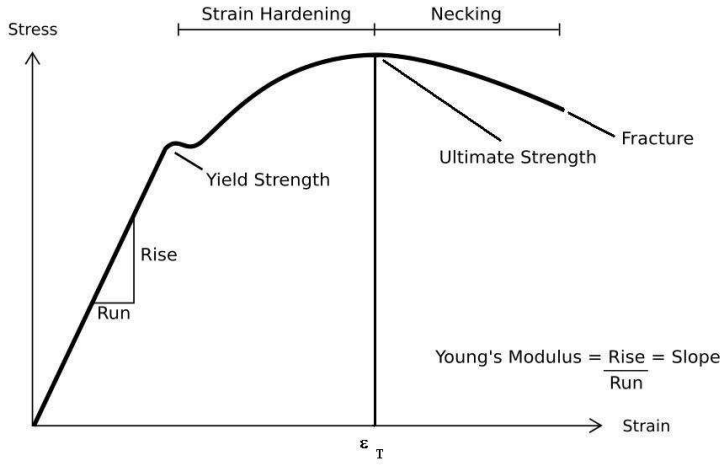

Figure 1.10. Stress-strain diagram [30]

The tensile stress and strain are determined in two different ways. In one, initial cross-sectional area and initial length are employed to calculate the stress and strain, respectively. This yields the engineering stress and strain. Nevertheless, the cross-section and length of the material change during tests. True stress and strain calculations account for the change in the dimensions. The shape of the stress-strain plot is similar after both calculations whereas the true stress-strain plot has an increasing trend after necking. The true stress-strain curve starting from the onset of plastic deformation till the point of necking can be approximated by the following formula relating the true stress (σ_t) and true strain (ε_T):

$$\sigma_T = K e_T^{\,n} \tag{1.1}$$

K is a constant and n is the strain hardening exponent which is defined as the measure of hardening and strengthening caused by the plastic deformation [30]. The strain hardening exponent is equal to the true strain at necking. Perfectly plastic solids have a value of n=0, while the elastic solids have a value of n=1.

It is also known that σ–ε behavior of materials is dependent on the loading (strain) rate [30]. This can be investigated by testing specimens in different pulling velocities which allows determining the strain-rate sensitivity (m) of materials. Strain-rate sensitivity shows the deformation behavior of the material. High strain-rate sensitive materials display

higher elongations, and low strain-rate sensitive materials show low elongations. Metals normally have low strain-rate sensitivity (<0,1) at room temperature; however, m increases with temperature. Superplastic materials, which show elongations between 100 and 1000 per cent, have high strain-rate sensitivity. This is because of their grain size or interphase spacing of 1 μm [31].

The tension and compression strength greatly depend on the selected material production technique. In cast state, magnesium crystals have random orientation. As a result, room temperature tensile and compressive yield strengths are usually equal [4]. The difference between the tension and compression strength can be based in different activation of deformation mechanisms in compression than in tension direction. This is based in the hexagonal lattice structure of the magnesium alloys [32]. Basically for wrought alloys, the mechanical properties depend greatly on the orientation of the flow patterns created during the working process. As an example, hot working tends to produce a desired crystal orientation of the basal plane. Also, the specimens taken parallel to the metal flow have higher tensile yield strength with lower compression strength. If a right angle is taken to the direction of the flow, the specimens will have higher compression strength but lower tensile yield strength.

Also, porosity greatly affects the strength of a material, as porosity decreases the effective area to carry the load and pores act as stress concentration spots within the part under loading. In order to produce materials with high tension and compression strength, the materials need to be porosity free. While the high-pressure-die-cast alloys have near zero porosity values, the typical porosity values for die-cast alloys are given in Table 1.5.

Table 1.5. Porosity of typical die-cast alloys [33]

	Porosity (Volumetric Per cent)
AM50	1,30
AM60	1,50
AZ91D	2,00

1.1.5.4. Corrosion Behavior. The corrosion of magnesium alloys is basically similar to that of other metals and depends on the similar factors that trigger corrosion of any metal. As magnesium is an electrochemically active material, the relative electro-potentials of the materials in contact are very important. In some environments, if there is no surface protection on a magnesium alloy, the part can be greatly damaged that's why magnesium alloys must not only be designed to meet the mechanical requirements but also the environmental factors, finishing, and assemblies [4].

1.1.5.5. Fatigue Behavior. In automobiles, nearly all parts are under cyclic loadings. Because of these types of loadings, parts will experience fatigue and will subsequently fracture. The fatigue affects parts life greatly, and so the parts should be designed according to the cyclic loadings occurring on the parts. Also, other factors such as corrosion and elevated temperatures, which are present in service environments of automobiles, greatly affect the fatigue behavior of magnesium alloys [34].

1.1.5.6. Creep Behavior. Creep is the permanent deformation of a solid material under constant loading at an elevated temperature. Creep occurs in long term exposure to levels of stress that are below the yield strength of the material at elevated temperatures. Magnesium is alloyed with elements which increase creep resistance of the alloy. In order to improve the creep resistance of the magnesium alloys, silicon, calcium, and rare earth elements are included in the alloying compositions [4].

1.2. Comparison of Magnesium Alloys with Competing Materials

Many structural materials are used in today's industry. In order to choose between these materials, the properties of these materials should be compared as each of these materials has some advantages and disadvantages. For the light duty commercial vehicle oil pans, the weight, strength, resistance to corrosion, and cost should be considered in the selection process.

As shown in Table 1.6, the ultimate tensile strength of the AZ91 die cast magnesium alloy (240 MPa) is lower than that of both the galvanized steel (320 MPa) and die cast aluminum 380 (324 MPa). However, the AZ91 die cast magnesium alloy has a yield strength (160 MPa) three times that of the plastic Dow Pulse 2000 (53 MPa) and possesses almost the same yield strength as the aluminum 380 (159 MPa). Moreover, the specific strength of the AZ91 die cast magnesium alloy (133 kNm / kg) is higher than both galvanized steel (41 kNm / kg) and Dow Pulse 2000 (48 kNm / kg). Also, magnesium alloys have high damping capabilities, which is an important feature for oil pans.

Furthermore, magnesium is a favorable metal for large area panel applications because of its higher performance in panel bendings. In Table 1.7, Ashby's performance indices [35] for stiffness and strength based design in bending are shown for steel, aluminum, and magnesium. As can be seen magnesium has a higher performance index, when compared with steel and aluminum.

Table 1.6. Comparison of selected mechanical and physical properties of various materials [36]

Material	**Cast Mg**		**Wrought Mg**		**Cast Iron**	**Steel**	**Cast Al**		**Wrought Al**		**Plastics (PC/ABS)**
Alloy/Grade	**AZ91**	**AM50**	**AZ80-T5**	**AZ31-H24**	**Class 40**	**Galvanized**	**380**	**A356-T6**	**6061-T6**	**5182-H24**	**Dow Pulse 2000**
Process/ Product	die cast	die cast	extrusion	sheet	sand cast	sheet	die cast	P/M* cast	extrusion	sheet	injection molding
Density (ρ, g/cm^3)	1,81	1,77	1,8	1,77	7,15	7,8	2,68	2,76	2,7	2,7	1,13
Elastic Modulus (E, Gpa)	45	45	45	45	100	210	71	72	69	69	2,3
Yield Strength (σ_y, Mpa)	160	125	275	220	N/A	200	159	186	275	235	53
Ultimate Tensile Strength (σ_{UTS}, Mpa)	240	210	380	290	293	320	324	262	310	310	55
Elongation (ε_f, per cent)	3	10	7	15	0	40	3	5	12	8	5 at yield and 125 at break
Fatigue Strength (σ_f, Mpa)	85	85	-	-	128	-	138	90	95	-	-
Thermal Cond. (λ, W/m.K)	51	65	78	77	41	46	96	159	167	123	-
Thermal Exp. Coeff. (α, mm/m-K)	26	26	26	26	10,5	11,7	22	21,5	23,6	24,1	74
Melting Temp. (T_m, ^{o}C)	598	620	610	630	1175	1515	595	615	652	638	143 (softening temp)

***P/M:Permanent mold**

Table 1.7. Ashby's performance indices for stiffness and strength based designs in bending [35]

Index → / **Material ↓**	**$E^{1/3}/\rho$**	**$\sigma^{1/2}/\rho$**
Steel	0,75	1,03
Al	1,52	2,51
Mg	2,00	3,29

The cost of magnesium is not competitive on per unit weight. However, when the comparison is made on volume basis, magnesium becomes comparatively better, see Table 1.8.

Table 1.8. Cost comparison of magnesium over with various materials [36]

Material	**Steel**	**Al**	**Plastics**	**Mg**
Cost ratio per unit weight	1	3,36	6,14	5,91
Cost ratio per unit volume	1	1,17	0,83	1,33
PCI for equal stiffness	1	1,67	3,74	2,22
PCI for equal strength	1	1,13	1,61	1,49

Also, for piece cost index (PCI), magnesium is very competitive. The predictions show that in the near future magnesium alloys will have lower prices and so become more competitive among the other contenders [36].

1.3. Magnesium usage in Automotive Components

In today's world, automotive industry has a considerable affection to magnesium alloys. Strict regulations take place in many countries to decrease the environmentally polluting emissions. Moreover, oil prices are increasing throughout the world, so more pressure is put on the automotive companies in order to increase the fuel efficiency of their cars. As magnesium alloys combine light weight and strength, these alloys are a preferable choice for automotive components. Also, the production rate of automotive components

needs to be high. Magnesium gives a 40-50 per cent increase in the production rate of automotive components, when compared with, for example, aluminum parts [36].

1.3.1. Interior Applications

As the corrosion is not a major concern in the interior of an automobile, magnesium has taken the place of steel in many applications in the interior of automobiles. These applications range from instrument panel, seat frame, and airbag housing to steering wheel. When an instrument panel is produced by integrating plastics, and steel components, the weight of these components will be as high as 30 kg; however, if the panel is produced from a single magnesium part, the total weight of this panel will come to a high value of 10 kg. Major producers of automobiles throughout the world such as GM, Ford, and Chrysler in USA, have utilized magnesium to decrease the overall automobile weight. Some of the parts that are used by the major automotive manufacturers are given in Table 1.9.

Furthermore, Alfa Romeo uses magnesium steering wheels to decrease the weight of this component [9]. Mercedes also uses magnesium in its seat structure in its SL roadster model [36]. For interior applications, magnesium alloys such as AZ91D, AM50A and AM60B can be recommended.

Table 1.9. Usage of magnesium parts by major automobile manufacturers [36]

Gobal Magnesium Applications in Automobiles					
System / Product	GM	Ford	Chrysler	Europe	Asia
Interior					
instrument panel	yes	—	ys	yes	—
knee bolster retainer	yes	—	—	—	—
seat frame	yes	—	yes	yes	yes
seat riser	yes	yes	yes	—	—
seat pan	—	yes	yes	—	—
console bracket	—	yes	—	—	—
airbag housing	—	—	yes	—	—
steering wheel	yes	yes	yes	yes	yes
keylock housing	yes	yes	yes	—	—
steering column parts	yes	yes	yes	yes	yes
radio housing	—	yes	—	—	—
glove box door	yes	—	—	—	—
window motor housing	—	yes	—	yes	—
Powertrain					
valve cover/cam cover	yes	yes	yes	yes	yes
4WD transfer case	yes	yes	—	—	—
manual transmission case	—	—	—	yes	yes
clutch housing & piston	yes	—	—	—	—
intake manifold	yes	—	—	yes	—
engine oil pan	—	—	—	yes	—
Alternator/AC bracket	—	—	yes	—	—
transmission stator	yes	—	—	—	—
oil filter adapter	yes	—	—	—	yes
electric motor housing	yes	—	—	—	—
Body					
door frame	—	—	—	yes	—
tailgate	—	—	—	yes	—
roof frame	yes	—	—	yes	—
sunroof panel	yes	yes	—	yes	—
mirror bracket	yes	yes	yes	yes	—
fuel filler lid	—	—	—	yes	—
door handle	—	—	—	yes	yes
Chassis					
wheel	yes	—	—	—	—
ABS mounting bracket	yes	—	yes	—	—
brake pedal bracket	yes	yes	yes	—	yes
brake/accelerator bracket	yes	yes	—	—	—
brake/clutch bracket	—	yes	—	—	—
brake pedal arm	—	yes	—	—	—

1.3.2. Engine and Powertrain Applications

Magnesium is a promising metal to be used in many automotive powertrain components as well as in the engine. Few examples of these components can be listed as follows: transmission cases, engine oil pans, clutch housing, intake manifold, and electric motor housing. Powertrain components require high stiffness, strength, corrosion resistance, and creep resistance in service. Some magnesium alloys such as AS21X and

AE42 are currently in use for powertrain components. One of the major manufacturers of magnesium powertrain components is GM, which uses magnesium alloys in most of its powertrain components. Volkswagen is another user of magnesium alloys (AS21 alloy) in its transmission case. Volkswagen has used AS21 alloy in such a high volume that has ever been used for an automotive component [26]. Also, the die-cast transmission case of Corvette is produced from magnesium alloys, which has a weight of 7 kg compared to 50 kg when this component to be produced out of steel [36]. Currently, the magnesium alloys Noranda AJ50X, Noranda AJ52X, and Dead Sea MRI-153 are considered for use in powertrain components for their elevated temperature creep resistance [26].

In recent years, Mg has also been used in the engine blocks in BMW sport cars [37]. Magnesium usage in engine blocks, which are previously manufactured previously from aluminum alloys, has reduced the weight of the engine by 15 per cent.

1.3.2.1. Light Duty Commercial Vehicle Oil Pans. Not a high number of magnesium oil pans have been introduced into the automotive industry. Still, Honda and a few European companies have used magnesium in their oil pan in recent years. Honda Insight oil pan has decreased the weight by 30 per cent, when compared to aluminum oil pans [10]. With the improved usage of all the light weight parts, Honda Insight has reached a 5,74 liter/100 km for a combined driving on the road for spark ignition engines [38]. As for the Ford transit I5 oil pan, which will be investigated in this thesis, the magnesium oil pan weighs 1,87 kg with the selected magnesium alloy which is a reduction of 45 per cent from the sheet drawn steel oil pan. By using magnesium in all the necessary parts of the vehicle, a great amount of reduction can be achieved. Still, the design requirements of the part should be met.

In automobiles the oil pans are positioned underneath the engine where it retains the engine's lubricating oil. It is bolted to the cylinder block underneath the engine. As the engine runs, the bolts transmit heat from the engine to the oil pan and the maximum service temperature reaches a high value of 140^{o}C. That's one of the reasons why the oil pans have been produced with materials such as steel or die-cast aluminum alloys which have high creep resistance. As a result, to produce a durable oil pan from a magnesium

alloy, the newly developed oil pan needs to have a good balance between the mechanical strength and resistance to corrosion

1.3.3. Body Applications

Magnesium is a preferable choice for body parts as magnesium sheet metal can reduce the weight of the body parts by greatly compared to steel. Magnesium body parts are especially preferable in door frames, and sunroof panels which work in bending. Other body parts made out of magnesium are door handles, roof frames, and mirror bracket.

Most of the body components manufactured from magnesium is used by European automobile companies [36].

1.3.4. Chassis Applications

Magnesium has limited usage in the chassis of the automobiles, as corrosion requirements for these components are relatively high, when compared with other parts in a vehicle. Magnesium alloys can be used in chassis components of mounting brackets, wheel, brake pedal arm, and the brackets which are used in the brakes. As the corrosion resistance is improved and the cost of the magnesium is decreased, magnesium alloys will be used in a higher volume in the chassis components [36].

1.4. Manufacturing Methods of Magnesium Alloys

Magnesium alloys can be shaped into any geometry using a range of manufacturing techniques. Mostly, magnesium alloys are produced by casting and forming methods. A method is chosen according to service requirements of a final product.

1.4.1. Casting of Magnesium Alloys

Casting is one of the basic production methods in the industry. Magnesium has a good castability, and when alloyed, casting properties of magnesium can be enhanced. Magnesium castings can be found in a variety of commercial products ranging from

computers, aerospace parts, automotive components, camera bodies, and portable devices, all of which require low weight and high stiffness. Similarly, low weight requirements necessitate the use of Mg alloys in a variety of automobile parts such as engine blocks, engine heads, push rods, pistons, and oil pans.

Casting is the production of parts by pouring of a molten metal into a preprepared cavity of a desired geometry and having the melt solidified in that cavity. The casting produces various geometries. Parts can have sizes ranging from a few millimeters to meters, and their weight can vary from a few grams to tons. Flexibility of design, ability of producing very small and very large parts, low cost, and suitability of mass production are a few of the advantages of the casting technique. These advantages give casting a distinct position over the other manufacturing methods.

Casting methods are widely used for producing parts from magnesium alloys. The choice of the casting method depends mostly on the application of the manufactured part, design requirements, and the volume of the production.

1.4.1.1. Permanent-Mold Casting. In permanent-mold (die) casting, a metal mold consisting of two or more parts is repeatedly used for the production of many castings of the same form. In the process, molten metal is poured into a cavity of a metal mold. After the molten metal is poured into the cavity, it’s allowed to solidify. In permanent-mold casting, the mold can be used many times before the mold wears out, which makes this method highly cost-effective.

The capability of producing multiple parts from a single mold is the greatest advantage of the permanent-mold casting method. This method is useful for high-volume production and is more suitable for casting parts with uniform wall thickness and limited undercuts. Also, another advantage of permanent-mold casting is that when compared with sand cast parts with tighter tolerances, a better surface finish, and higher mechanical properties can be attained. A disadvantage of permanent-mold casting is the high porosity concentration in the parts. Typically 2 per cent porosity generates in permanent-mold castings as given in Table 1.5.

Various parameters affect the casting process. Mainly, in permanent mold casting, selection of mold materials, mold coatings, mold temperature, cooling rate, and pouring temperature have a great effect on the quality of the final product.

Firstly, the material of the mold affects the mold life and the cooling rate of the melt. Ferrous metal molds should be used for casting magnesium alloys, as molten magnesium does not attack ferrous metal molds. The most commonly used mold material is gray cast iron for permanent mold castings of magnesium alloys. These molds are durable molds which can obtain more than 100,000 castings per mold. The basic disadvantage of these molds is the low surface quality. For the parts which require extensive machining gray cast iron molds can be used effectively [39].

Secondly, the internal coating on the molds serve as a barrier between the molten metal and the surface of the mold as the metal solidifies. These coatings are used to prevent premature freezing of the melt, control the rate and direction of the casting solidification, minimize the thermal shock of the mold material, prevent soldering of molten metal to the mold, and vent air trapped in the mold cavity. In order to gain these advantages, basically two types of coatings are used: insulating and lubricating. These coatings should be selected according to material to be cast. Lubricating coatings are generally used for magnesium alloys [39].

Moreover, the mold temperature affects the mechanical properties and quality of a cast part. In order to meet the specifications required from the cast part, mold temperature should be determined according to variables such as pouring temperature, cycle frequency, casting weight, casting shape, casting wall thickness, mold wall thickness, and the thickness of mold coating. Other than these factors, preheating of the mold should also be done in order to reduce the casting defects within the parts.

One other parameter affecting the casting is the cooling rate of the melt. High cooling rates in permanent mold castings refine the grain size of the alloys in contrast to the coarsening of the grain size with the low cooling rates [40].

Lastly, the melt to be cast should have an optimum pouring temperature to obtain a high quality casting. If pouring temperatures of the melt is low, the melt will solidify too rapidly and that will cause porosity, poor casting details, and interrupted directional solidification. These will lower the mechanical properties of the parts. If the pouring temperature of the melt is high, the mold will have warpage which will result in loss of dimensional accuracy. Basically, the optimum pouring temperatures for magnesium alloys are suggested to be between 705 and 790 ^{o}C (T_m=650^{o}C for magnesium) [39].

All these variables influence the microstructure of the permanent cast parts. Most metallurgical alloys have a dendritic structure in a mold. Also, columnar and equiaxed dendrites are usually present in the casting. In the periphery of the mold, the equiaxed chilled zone develops as the liquid metal is poured. At the center of the mold equiaxed dendritic crystals are mostly present [39]. The solidification of a material in permanent mold is shown in Figure 1.11 [39]. Furthermore, the permanent mold cast magnesium alloys have large amounts of divorced, partially coupled, and coupled eutectic phases [4, 41].

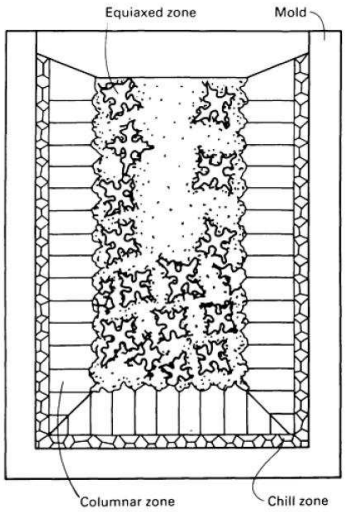

Figure 1.11. Solidification of melt in permanent-mold [39]

The alloys used are same for permanent-mold casting and sand casting, with the exception of ZK series. In the automotive industry, permanent-mold casting is used to produce engine blocks, front engine covers, etc [42].

For comparison, the mechanical properties of alloys produced via permanent-mold casting and other methods are given in Table 1.10. The results of the mechanical properties show that permanent-mold casting has similar properties when compared to other casting methods.

Table 1.10. Mechanical properties of production methods [4]

Process	**σ_{UTS}, MPa**	**σ_y, MPa**	**δ, per cent**
Permanent-mold casting	212-230	140-159	3.0-5.6
Sand casting	200-215	138-146	3.0-6.0
Investment Casting	256-272	195-212	5.0-9.0
HPDC	200-250	140-160	3.0-5.0
Thixomolding	190-241	140-160	3.0-5.0
Squeeze casting	270-290	207-225	5.0-13

1.4.1.2. Sand Casting. In sand casting, molten metal is poured into a cavity in a mold produced of a sand mixture. After the metal is poured into the cavity, it's left for cooling to solidify the molten material. For magnesium alloys, green sand is mostly used as sand mixture for preventing the bonding between the molten material and the mold. The greatest advantage of using sand casting technique is that parts with various sizes can be cast with low cost [4].

1.4.1.3. Investment Casting. Investment casting has been used for years for producing automotive components. In investment casting, ceramic slurry is applied around a disposable pattern which is then allowed to form a disposable casting mold. Afterwards, the liquid material is poured into this mold and left to solidify. After the part has solidified, the casting is removed from the mold. The mold is destroyed during the removal of the casting. Lastly, finishing and inspection is done on the casting.

1.4.1.4. High-Pressure Die Casting (HPDC). High-pressure-die-casting (HPDC) is used in high volume production for producing a variety of geometries from magnesium alloys. Most of the parts produced from magnesium alloys are produced by this manufacturing

method because of its fast production rates and the ease of automation. Furthermore, magnesium alloys are very suitable for this manufacturing method. The alloys have high fluidity; thus thin walled parts (2 mm) can be easily cast with this method. The parts produced by the high-pressure-die-casting process have excellent dimensional properties and smooth surfaces, that's why the final products require almost no machining. These advantages make high pressure die cast magnesium alloys a good choice for automotive manufacturers [28].

1.4.2. Semi-solid production methods

1.4.2.1. Thixomolding. Thixomolding is one of the most researched subjects among the magnesium alloy production methods. In thixomolding, a magnesium alloy is heated into a semi-solid state, which then is injected into a mold cavity to solidfy. Thixomolding is a cost effective manufacturing method as the process requires lower operating temperatures. Thixomolding cast parts are used in cameras, cell phones, and as well as in shift cams in Ford transmission and seat components [38]. The thixomolded parts can have thinner wall sections, and a 50 per cent reduction in porosity is possible. The semi-liquid material during production is protected from oxidation at high temperatures by using argon shield gas.

1.4.2.2. Squeeze Casting. Squeeze casting is a process in which casting and forging processes are combined into one single process. In this method, the molten magnesium alloy is poured into bottom half of the die. As the molten alloy starts to solidify, the upper part of the mold closes to apply pressure on the molten alloy. Using squeeze casting, complex geometries can be produced with low porosity and improved mechanical properties.

1.5. Production Cost of Magnesium

The market for magnesium alloyed automotive parts has increased about 15 per cent each year since 1990's [43]. As the oil prices and environmental concerns have increased, a similar market growth for magnesium alloys is expected in the future. As can be seen in Figure 1.12, the growth of magnesium usage increased steadily till 2004.

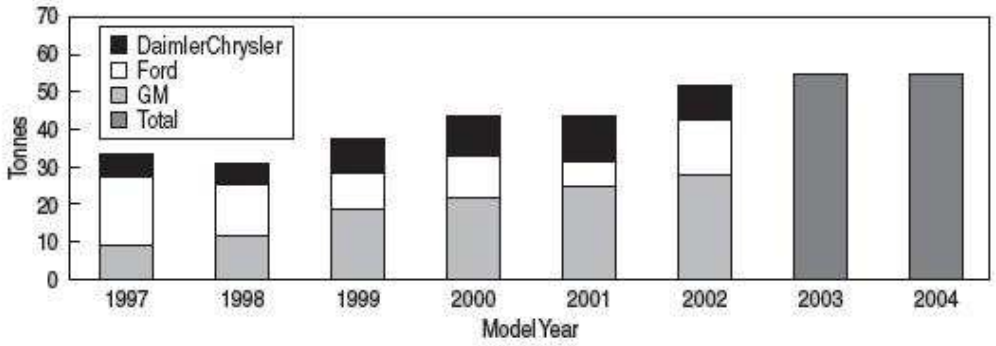

Figure 1.12. Projected growth of magnesium usage

By 2004 the magnesium usage in USA had increased to 58,000 tons [43]. It is still expected to grow steadily. Estimations show that magnesium usage will increase with the increase of the use of cheap raw magnesium from China [43].

The price of unalloyed magnesium ingots in 2002 was $1,2/lb compared to $0,65/lb for unalloyed aluminum. As already given in Table 1.9, on per-pound bases, magnesium costs 1.8 times higher than aluminum; however, on a volume basis, it costs only 1.2 times higher. That's why the performance of the materials and the density of materials are required to be included for a cost comparison.

The metallurgical production of magnesium depends mainly on two techniques, electrolysis and thermal reduction as already stated previously. Electrolysis is the older technique and accounts for 80 per cent of the magnesium production. The thermal reduction is a cost efficient technique as it uses less energy, when compared with the other techniques. However, the high cost of cell feed preparation and the low production rates are major disadvantages of this technique. The operational costs of electrolysis technique are relatively lower than thermal reduction. The cost varies for electrolysis between $0,60/lb and $0,99/lb. In contrast, it's between $0,93/lb and $1,19/lb for thermal reduction. The analysis of the operational costs of magnesium products is given in Figure 1.13 [43].

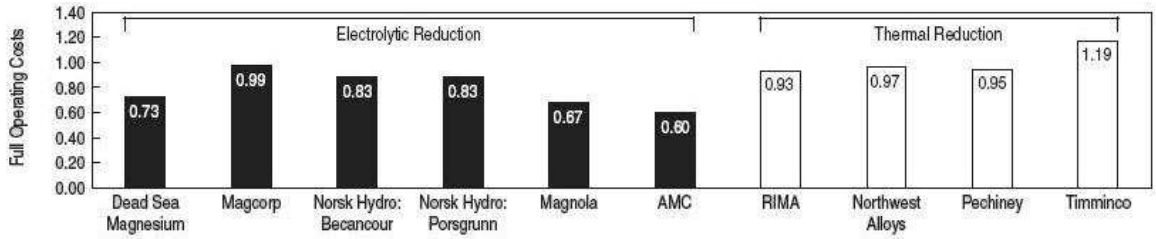

Figure 1.13. Operational costs of electrolysis and thermal reduction techniques based on several companies [43]

The full cost of magnesium production includes the labor, energy, capital, and material costs. Also, the full cost varies with the production volume capabilities of the plants. The fixed costs decrease as the volume of the production of the plant increases. The full cost comparison between electrolysis and thermal reduction is given in Figure 1.14 [43].

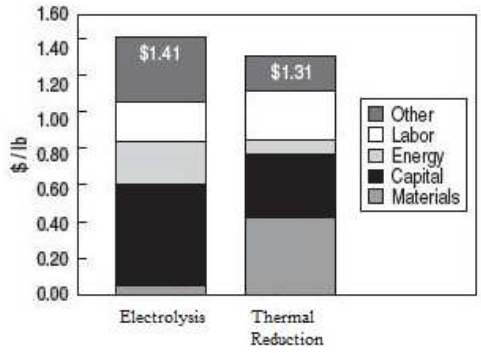

Figure 1.14. Analysis of full costs [43]

According to the full cost comparison, electrolysis is more expensive than thermal reduction, mainly due to the high capital and much lower materials cost [43].

2. OBJECTIVES

The primary objectives of the current research are:

- To develop magnesium alloy compositions based on Mg, Al, Si, and Ca suitable for automotive oil pans in light duty trucks.
- To determine the tensile and compressive strength of the magnesium alloys developed.
- To compare and contrast the findings of this research to those available in the literature and hence to assess the possibility of developed experimental alloys to be used for oil pans.

3. EXPERIMENTAL PROCEDURES

3.1. Alloy production: Permanent – mold casting

In this study, four magnesium alloy compositions possibly suitable for light duty truck oil pans have been investigated. After, a literature survey to cover the present knowledge on magnesium alloys and the automotive parts that have been produced by magnesium alloys, the four magnesium alloy compositions have been selected based on the AS21 and ACM522. The experimental alloys in the current thesis work are composed of Mg, Al, Si, and Ca. These elements are a combination of those present in AS21 and ACM522. Specifically, the ACM522 alloy is the only magnesium alloy used for serial production of oil pans. The alloying composition of the AS21 and ACM522 is given in Table 3.1.

Table 3.1. Experimental magnesium alloy compositions

Alloy	**Mg**	**Al**	**Si**	**Ca**	**Mn**	**Zn**	**Ce**
	weight per cent	**weight per cent**	**weight per cent**	**weight per cent**	**weight per cent**	**weight per cent**	**weight per cent**
AS21	96,36	2,30	1,13	0,00	0,19	0,02	0,00

ACM522	90,70	5,00	0,00	2,00	0,30	0,00	2,00

Due to limited experimental resources (material and equipment) and for ease of comparison, Al and Si amounts are kept constant whereas the amount of Ca is varied. As explained in section 1.1.4, it is aimed to have alloys with different Ca/Al ratios to assess the formation potential of Al_2Ca phase along with other intermetallic phases and then to investigate the influence of those phases in the mechanical properties studied in this thesis. The selected compositions are given in Table 3.2.

Table 3.2. Experimental magnesium alloy compositions

Alloy #	**Mg**		**Al**		**Si**		**Ca**		**Ca/Al wt per cent / wt per cent**
	weight per cent	**atomic per cent**	**weight per cent**	**atomic per cent**	**weight per cent**	**atomic per cent**	**weight per cent**	**atomic per cent**	
1	96,1	96,7	2,0	1,8	1,2	1,1	0,7	0,4	0,35
2	95,8	96,5	2,0	1,8	1,2	1,1	1,0	0,6	0,5
3	95,2	96,2	2,0	1,8	1,2	1,1	1,6	1,0	0,8
4	94,8	95,9	2,0	1,8	1,2	1,1	2,0	1,2	1,0

Alloys have been produced via permanent-mold casting. Firstly, magnesium and aluminum have been put into a crucible made of steel with a capacity of 100 kg. Then the crucible has been heated up to 800^{o}C to melt the materials within it. After magnesium and aluminum have been melted, calcium and silicon have been added to the crucible in predetermined amounts based on the alloy composition. Through the melting processes a protective blanket, which is composed of potassium chloride, magnesium chloride, calcium chloride, and sodium floride, has been used to protect molten magnesium alloy from oxidizing. When all the elements have been melted and mixed, the molten material has been poured into a cylindrical steel mold to produce rods with 23 mm in diameter and 300 mm in length. The mold has a wall thickness of 50 mm and has been preheated to

250-280^{o}C. The casting has been repeated for each composition for 6 times, which has produced 6 rods for each alloy. Then, the solid alloy rods have been cut into 100 specimens with a diameter of 23 mm and a length varying between 70-73 mm.

3.2. Microscopical Analysis

After the alloys have been cast, two specimens have been selected from each of the alloys to check the compositional homogeneity within a particular specimen and also the compositional match between the specimens of a particular alloy group. From one of the selected specimens, two semi-cylindrical samples have been taken from each end (top and bottom). These samples have been used to confirm the homogeneity within the specimen. From the other selected specimen, one semi-cylindrical sample has been taken from one end. This sample has helped to confirm the compositional match between the two selected specimens for the particular alloy.

For the preparation of the sample surface for chemical analysis, firstly, each sample has been hot mounted in bakelite. Then wet grinding on silicon carbide paper discs of 120, 240, 320, 400, and 600 grits has been done sequentially. The remaining residues left over the samples have been flushed off using streaming water after each grit of the abrasive paper. No etching has been done on these samples. After the grinding operation has been completed, EDS (Energy Dispersive Spectroscopy) technique has been used to confirm the composition of the samples. The EDS results have suggested that alloy preparation has produced the specified alloy compositions given in Table 3.2.

Next, to determine the phases present in an alloy and investigate the composition of the phases, the samples used for EDS analysis have been metallographically prepared for microscopy. A suspension of 15, 10, 5, 1, 0,5, and 0,03 μm sized alumina powder and water has been applied sequentially on a polishing cloth to polish the sample surface. Each of the samples has been polished on the polishing cloth till no visible scratch has been left over the sample surface. The remaining residues left over the samples have been flushed off using streaming water after each polishing operation.

After grinding and polishing operations have been finished, Toluol has been used to clean the surface of the specimens. Lastly, the microstructural images have been taken by using Nikon Eclipse LV150 microscope with maximum magnification of 1000x connected to a computer that ran Clemex Captiva 4.0 imaging software [44]. ESEM (Environmental Scanning Electron Microscope) photos have been also taken as needed. Then, the compositions of the phases present in the microstructures have been investigated by the EDS with a beam diameter of 5 μm. No etchant has been used on the surface of the samples for imaging the particles as they have been already visible under the microscope without etching.

After the EDS analysis, the amount of phases and porosity present in the samples has been determined with the image processing and analysis software IMAGEJ [45].

Lastly, the grain structure has been imaged by using the light microscope. An etchant with the composition of 2 mL HF (48%), 2 mL HNO_3 (conc), and 96 mL H_2O has been used to reveal grain boundaries [41]. After etching has been finished, Toluol has been used to clean the surface of the specimens.

3.3. Tensile Testing

Tensile testing has been performed according to ASTM E8M – 00b (METRIC) Standard Test Methods for Tension Testing of Metallic Materials [46]. For tensile testing, small size specimens have been selected based on this specification. The shape of the tensile testing specimen is given in Figure 3.1.

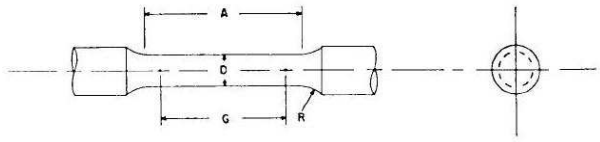

Figure 3.1. Tensile testing specimen

The selected specimen has a gage length (G) of 30,00 mm, diameter (D) of 6,00 mm, fillet radius (R) of 6,00 mm, reduced section length of 36,00 mm, and a total length of 70,00 mm. A photograph of a specimen is given in Figure 3.2.

Figure 3.2. Specimen used in tensile testing

The gap between the jaws of the testing machine are greater than the diameter of the specimens; that's why two screw grips have been produced with 20 mm diameter and 150 mm length. These grips have 15 mm deep, 12 x 1,5 metric threaded holes in one side to attach the specimens.

In order to conduct the tests, firstly, the gage length of 30 mm has been marked along the gage length of the specimens. After marking of the specimens and screwing of the specimens into the holders, the holders have been gripped into the jaws of the machine. Then an extensometer has been clamped onto the tension specimen.

The tests have been done using a computer controlled, 100,000 N Mares tension / compression testing unit. After the necessary parameters have been typed into the program, the tests have been started.

A total of 16 specimens from 4 different alloy compositions have been used for tensile testing. Four specimens have been used from each alloy. Two specimens have been tested at a given test speed. The tests have been done using two speeds 1 mm/min and 10 mm/min, with a preload of 5 kg. The tests have continued till the fracture.

3.4. Compression Testing

Compression testing has been performed according to ASTM E9 – 89a (Reapproved 2000) Standard Test Methods of Compression Testing of Metallic Materials at Room Temperature [47]. Medium size specimens suggested by this specification have been selected. The selected specimen has a diameter of 20,00 mm, length of 60,00, and a length-to-diameter ratio of 3,00. A photograph of a specimen is given in Figure 3.3.

Figure 3.3. Specimen used in compression testing

In order to conduct the tests, firstly, a gage length of 30 mm has been marked on the specimens. Then the specimen has been placed on the compression stand. Both ends of the cylindrical specimen have been greased to minimize the friction and to avoid barreling.

Then an extensometer has been clamped onto the compression specimens. A protective shield has been installed to contain the specimen. The tests have been done in the same machine used for tensile testing.

A total of eight specimens from four different alloy compositions have been used for compression testing. Two specimens have been tested from each alloy. The compression testing has been carried out with 5 mm/min velocity. The tests were done with a preload of 5 kg. The tests were continued till the specimens have either fractured or buckled.

After the mechanical property determination, the composition that yielded the best properties and hence thought to be the most suitable one for oil pans, has been selected to assess the eligibility of the alloy by CAE (Computer Aided Engineering) for the light duty truck oil pans.

3.5. CAE Analysis

CAE analysis for comparing the modes of a light duty truck (Ford Transit I5) oil pan produced from magnesium has been investigated using Hypermesh [48]. Modal analysis has been performed to compare the natural frequencies and the corresponding mode shapes of these two structures as the most important characteristic of the oil pan is its damping capacity.

The oil pan has been structured using 1^{st} order quadrilateral elements with size of 3 mm in order to have a better resolution for the mesh. The analysis has been carried out

for two materials, steel and the alloy 4 developed in this study. The thickness of the steel oil pan is 1,3 mm overall. The thickness of the magnesium oil pan is 8 mm and the flange of it is 3 mm. The steel oil pan has the properties of E of 210 GPA, ρ of 7,9 g/m^3, and mass of 3,36 kg and magnesium oil pan has the properties of E of 45 GPA, ρ of 1,78 g/m^3 , and mass of 1,87 kg.

In order to simulate the service conditions of the oil pan, fixing points on the oil pan to the engine block are constrained in all degree of freedom and a point mass weighed 50 g is hung by rigid elements for simulating the bolts.

4. RESULTS AND DISCUSSIONS

4.1. Microscopic Analysis

The permanent-mold cast alloys produced in this thesis work exhibit a grain size in the range of 5-10 μm. A representative grain microstructure for the alloys, as revealed by light microscope, is shown in Figure 4.1. The usual die cast microstructure shown in Figure 1.11 is not observed because of the die-preheating and thick die walls. The grain size does not vary with increasing calcium content. Nevertheless, Ca seems to refine the grain size as a larger size (27,5 μm) has been reported [49] for a similar alloy with lower (0,25 weight per cent) Ca content than that used in the alloys of the current study.

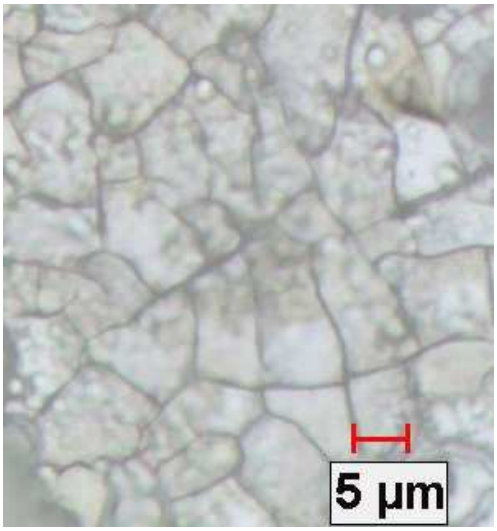

Figure 4.1. Grain structure of the alloy 3

Metallographic analysis of the developed alloys by light microscope shows that each alloy composition displays distinct phase morphologies. The only phase observed by the light microscope in all the alloys is identified to be an intermetallic phase Mg_2Si, routinely formed in silicon containing magnesium alloys. The Mg_2Si intermetallic compounds can be easily distinguished by their light blue color under light microscope.

The intermetallic compound Mg_2Si that has a face centered cubic crystal structure [32] appears in two morphologies, polyhedral and the Chinese script. The Chinese script morphology forms during the solidification of the hypoeutectic alloy melt. As the melt cools below the liquidus temperature, first Mg-Al-Si solid solution grains form. Continuation of the solidification creates cored grains; a concentration gradient of Al and Si develops from the core (low content) to the periphery (high content) of the grains. When the eutectic temperature is reached, a binary eutectic Mg_2Si+(Mg-Al-Si) forms with the transformation $L \rightarrow \alpha + Mg_2Si$, where L is the liquid and α is the Mg-Al-Si solid solution matrix. This transformation path leading to the appearance of the Chinese script Mg_2Si is also reported by Kim et. al. [49]. Interestingly, Bronfin et. al. [50] claim that cooling the hypoeutectic melt results in the polyhedral Mg_2Si morphology, which the author of this thesis does not agree with because polyhedral Mg_2Si particles should be the proeutectic phase as will be explained later. The reason for development of the Chinese script morphology is in fact the difference in the growth modes of the matrix and the Mg_2Si phase. It is apparent from the polyhedral morphology of Mg_2Si particles that this phase is a

faceted one, while the matrix is non-faceted. Eutectic growth of such non-faceted/faceted systems is irregular in shape, similar to the Chinese script morphology and unlike the regular lamellar eutectic morphology [51].

The polyhedral Mg_2Si forms as a proeutectic phase. This can occur only when the melt concentration is greater than the eutectic composition. Knowing that the eutectic composition is 1,34 weight per cent for Mg-Si system and that the Si content of studied alloys in this current work is 1,2 weight per cent, the proeutectic Mg_2Si formation is only possible if the melt is enriched beyond the eutectic composition. Conversely, depression of the eutectic point can also lead to proeutectic phase formation. Indeed, it has been reported that Al additions depress the eutectic temperature and reduce the eutectic composition [49]. Also, the solidification enriches the melt with respect to Al and Si. In addition, calcium which is present in the currently studied alloys is found to decrease the eutectic transformation temperature [52]. These effects expand the liquid plus Mg_2Si phase field which promotes the polyhedral, proeutectic Mg_2Si particles. The formation of this phase may also be a result of divorced eutectic growth, where nucleated Mg_2Si particles get engulfed by the matrix [51]. The hypereutectic liquid in equilibrium with the proeutectic Mg_2Si particles can solidify into the Chinese script Mg_2Si morphology below eutectic transformation temperature.

The concentration of 1,1 weight per cent Si is observed to give fine Chinese script like phases [13]. It is also reported in the same reference that the Si amount greater than 1,4 weight per cent increases the amount of coarse Chinese scripts. This is the reason for the formation of fine Chinese script Mg_2Si phase as the composition of the alloys in this current work is 1,2 weight per cent. The increase of the Ca content in the composition of the alloy, however, increases the thickness of the phases.

The alloy 1, which contains the lowest Ca concentration, consists of connected short rods forming the Chinese script phase morphology as seen in the central region of the microphotograph shown in Figure 4.2. It is also worth seeing that free ends of the rods (not connected to other rods) are attached to a blocky particle. Also, a few unattached blocky ones are scattered around the before mentioned features. These blocky particles have formed via the mechanisms explained above.

The amount of the Mg_2Si phase determined using the microphotos is 2,65 area per cent which is the lowest among the four alloying compositions as seen in Table 4.1.

Table 4.1. The amount of Mg_2Si and Mg-Al-Ca phases and porosity in the alloys

Alloy	**Mg_2Si (area per cent)**	**Mg-Al-Ca Phases (area per cent)**	**Porosity (area per cent)**
1	2,65	1,8	3,5
2	3,85	2	5
3	4,15	2,1	6,6
4	6,25	2,3	4

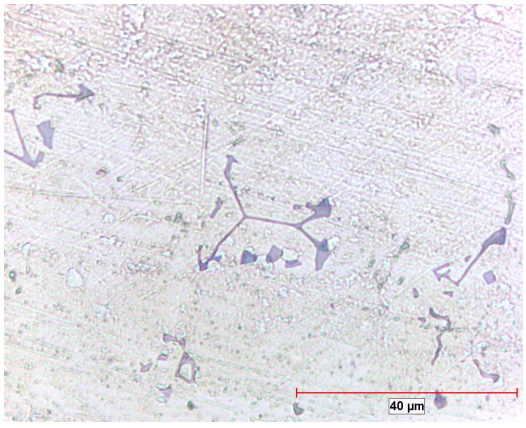

Figure 4.2. Microstructures of the alloy 1

Analysis of the alloy 2 shows that the Mg_2Si particles are mostly in blocky morphology; few short fiber-like ones and ones with Chinese script morphology have also been seen. A representative microphotograph for the alloy 2 is given in Figure 4.3. The addition of Ca seems to promote the formation of Mg_2Si phase; amount of the Mg_2Si phase has increased to 3,85 area per cent.

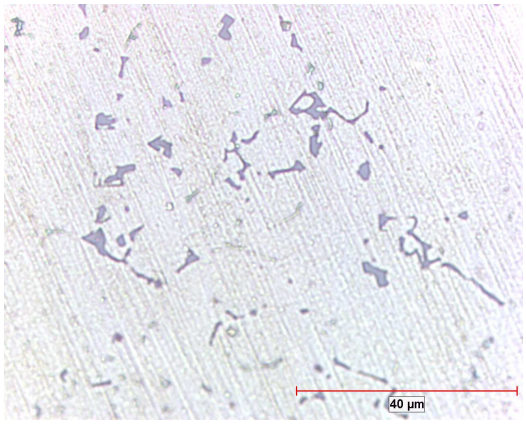

Figure 4.3. Microstructures of the alloy 2

Metallographic analysis of the alloy 3 shows that the alloy has more Mg_2Si Chinese script phase. A representative microphotograph of the alloy 3 is seen in Figure 4.4. In addition, a small number of blocky phases can be seen, as well. The Chinese script phase has a faceted while the matrix has a non-faceted structure. As the specific energy between the faceted/non-faceted phases is anisotropic, these irregular structures form [53]. These crystallographic orientations occur between these phases in order to minimize the interfacial energy. Amount of the Mg_2Si phase has increased to 4,15 area per cent in the alloy 3.

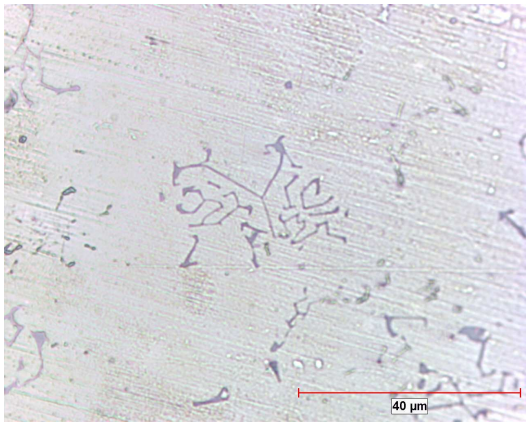

Figure 4.4. Microstructures of the alloy 3

The alloy 4 shows similar phase features to the alloy 1. However, one major difference is that short rods are emerging from diamond and trapezoid shaped particles as

seen at the central region of Figure 4.5. These diamond shaped polyhedral particles cover a larger area in the microstructure of the alloy when compared with the other three alloys. In addition, features as seen in the alloy 1 are also present in the alloy 4. One such feature is seen towards upper-left corner of Figure 4.5. Also, smaller blocky particles are present around these rod-attached large diamond features. Amount of the Mg_2Si phase has increased to 6,25 area per cent, which is the highest among the four alloying compositions. This increase may be reasoned to the presence of Ca, which not only promotes the formation of more Mg_2Si phase, but also polyhedral (blocky) morphology.

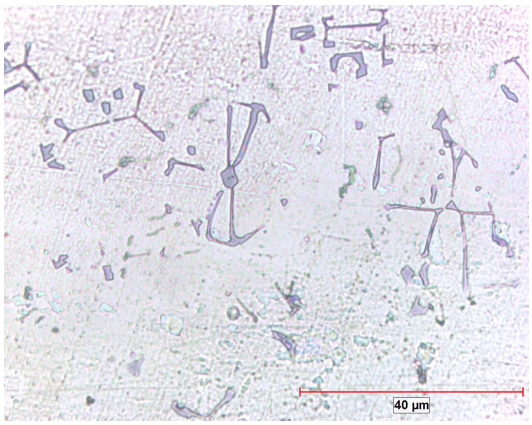

Figure 4.5. Microstructures of the alloy 4

The length of the Chinese script like phases and the short rods emerging from diamond shaped particles varies from 5 to 30 µm. As the grain size varies between 5 and 10 µm, the phases extend through the grain boundaries to neighboring grains, pinning them in place and increasing the mechanical properties of the alloys. This results in an interconnected network of grains held together by the Chinese script Mg_2Si phases. That's why the morphology of the Mg_2Si phase has been found to be critical to the mechanical properties of the alloys.

Not all of the phases that are present in the microstructure of the alloys could be observed using the light microscope. Especially, the phases that contain higher Al and Ca percentages cannot be observed. These phases have been investigated using an ESEM to analyze the composition of the phases and to take the microstructural images of the alloys.

Microstructures have been taken at 1500x, 3000x, and 6000x magnification with 20 kV beam.

BSE (Back Scattered Electron) analysis has been used in order to differentiate the phases by their color contrast which is sensitive to phase compositions. BSE uses raster scanning pattern with a high-energy beam of electrons. The electrons interact with the atoms in the sample. Back-scattered electrons are then reflected by elastic scattering thus producing signals that contain information about the phases. As the intensity of BSE is dependent on atomic weight and ionization energy of the substance investigated, these two parameters play an important role in the color of the phase observed in the BSE image. Aluminum has an ionization energy of 577,5 $kJmol^{-1}$ and atomic weight of 26 $gmol^{-1}$, calcium has an ionization energy of 589,8 $kJmol^{-1}$ and atomic weight of 40 $gmol^{-1}$, and silicon has an ionization energy 786 $kJmol^{-1}$ and atomic weight of 28 $gmol^{-1}$. Silicon has the highest ionization energy, that's why it has the darkest color in the BSE photos when compared with aluminum and calcium. Calcium has the lightest color in the BSE photos. Indeed, calcium has a lighter color than aluminum as it has a higher atomic weight than aluminum [54].

Mg-Al-Ca ternary systems have been expected to develop Laves phases of Mg_2Ca, Al_2Ca, and β-$Mg_{17}Al_{12}$ [18]. Also, $(Mg,Al)_2Ca$ have been expected to form within the Mg-Al-Ca matrix [55]. These intermetallic phases form after the primary α-Mg solidification occurs. The morphology of the β-$Mg_{17}Al_{12}$ phase is round and Mg_2Ca and Al_2Ca are dendritic and blocky [50]. These phases form later than the Mg_2Si phase due to the slow diffusion rates of Al and Ca in solid Mg [50]. The EDS analysis has been conducted on the samples to verify if any phase observed by the BSE has the composition of Laves phases. The β-$Mg_{17}Al_{12}$ Laves phase has been observed within this thesis work.

The BSE analysis has shown that the phases that couldn't be observed with the light microscope have light color. These phases seem to be distributed around the Mg_2Si phases. In previous analyses, aluminum enrichment for similar alloys is found near the Mg_2Si phases [56]. This is the result of the creation of compositional gradients during solidification and the production of a cored structure as explained previously. The grain interior contains less solute aluminum.

Chemical compositions gathered by the EDS analysis for different phases for the four compositions can be seen in Table 4.2. The first number on the label indicates the alloy number, and the second number indicates the phase number present in the image. These chemical compositions are only qualitative due to the beam diameter of the ESEM machine. The EDS analysis can be conducted on a spot of about 5 μm diameter, which is larger then some phases analyzed. Nonetheless, the EDS analysis indicates that phases other than Mg_2Si are present within the Mg-Al-Si-Ca matrix.

Table 4.2. Chemical compositions of phases

	Mg		Al		Si		Ca	
Label	weight per cent	atomic per cent	weight per cent	atomic per cent	weight per cent	atomic per cent	weight per cent	atomic per cent
Alloy 1 - 1	91,36	92,47	1,26	1,15	7,06	6,18	0,33	0,20
Alloy 1 - 2	88,44	89,95	0,87	0,80	10,52	9,25	0,17	0,10
Alloy 1 - 3	84,86	88,08	1,44	1,35	7,22	6,49	6,47	4,08
Alloy 2 - 1	73,50	78,65	0,98	0,95	13,87	12,85	11,64	7,56
Alloy 2 - 2	74,50	76,59	24,80	22,97	-	-	0,70	0,44
Alloy 2 - 3	75,43	78,02	1,28	1,19	23,08	20,66	0,21	0,13
Alloy 2 - 4	74,39	76,32	25,61	23,68	-	-	-	-
Alloy 3 - 1	82,45	84,44	2,05	1,89	15,22	13,49	0,27	0,17
Alloy 3 - 2	68,62	70,97	27,56	25,68	3,56	3,19	0,26	0,17
Alloy 4 - 1	79,92	82,11	0,95	0,88	19,13	17,01	-	-
Alloy 4 - 2	83,99	85,85	1,82	1,67	13,92	12,31	0,28	0,17
Alloy 4 - 3	80,91	83,06	2,11	1,95	16,58	14,74	0,39	0,25
Alloy 4 - 4	77,10	78,89	22,90	21,11	-	-	-	-
Alloy 4 - 5	81,34	84,99	2,38	2,24	9,07	8,20	7,21	4,57

In the alloy 1, the Chinese script like phases with blocky particles at the end of the fibers can be seen in the BSE photos. In order to investigate the composition of these

phases an EDS analysis has been conducted on the fibers (mark 1: Alloy 1-1 in Table 4.2) and the blocky particles (mark 2: Alloy 1-2 in Table 4.2) of this Chinese script like phase in Figure 4.6. According to the EDS analysis, the fiber of the Chinese script like phase (mark 1: Alloy 1-1 in Table 4.2) is composed of Mg, Al, Si, and Ca. This phase has a dark color indicating a high Si concentration. However, the measured Si is only 7,06 weight per cent. Note that the fiber of the Chinese script has a thickness of about 1 µm. As the beam diameter is 5 µm, Al and Ca (in the matrix) around the Chinese script phase have been also read in the EDS analysis showing a reduced Si content.

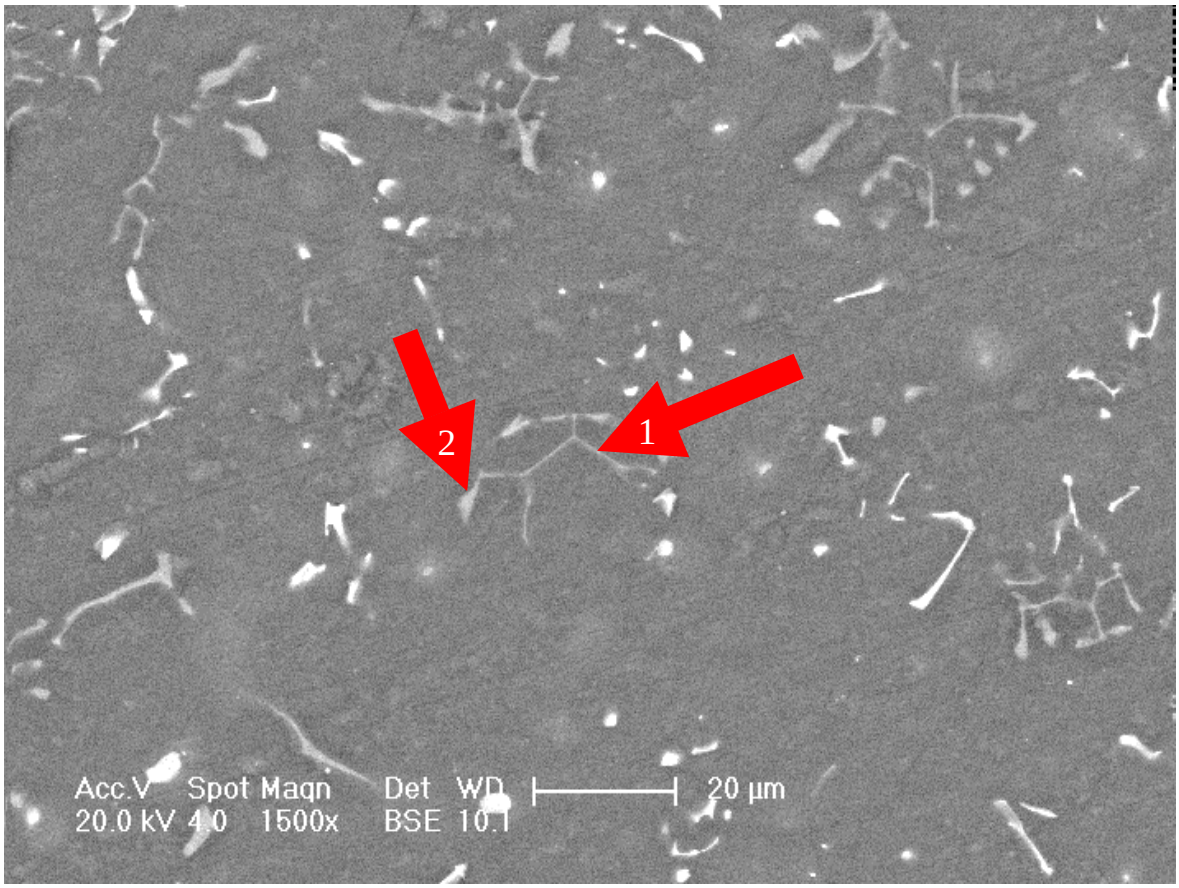

Figure 4.6. A BSE image of the alloy 1

This phase should therefore be of Mg_2Si composition due to its dark color. The blocky particle (mark 2: Alloy 1-2 in Table 4.2) at the end of the fiber has a higher Si (10,52 weight per cent) concentration with very low Al and Ca concentrations. This particle is larger than the fiber (mark 1). That's why less Al and Ca have been read from the

periphery of the phase. Both the arms and blocky particles hence should be Mg_2Si. In Figure 4.6, the white colored phases that are not marked have been analyzed, as well. The white phases are composed of Mg, Al, and Ca. These phases are possibly β-$Mg_{17}Al_{12}$.

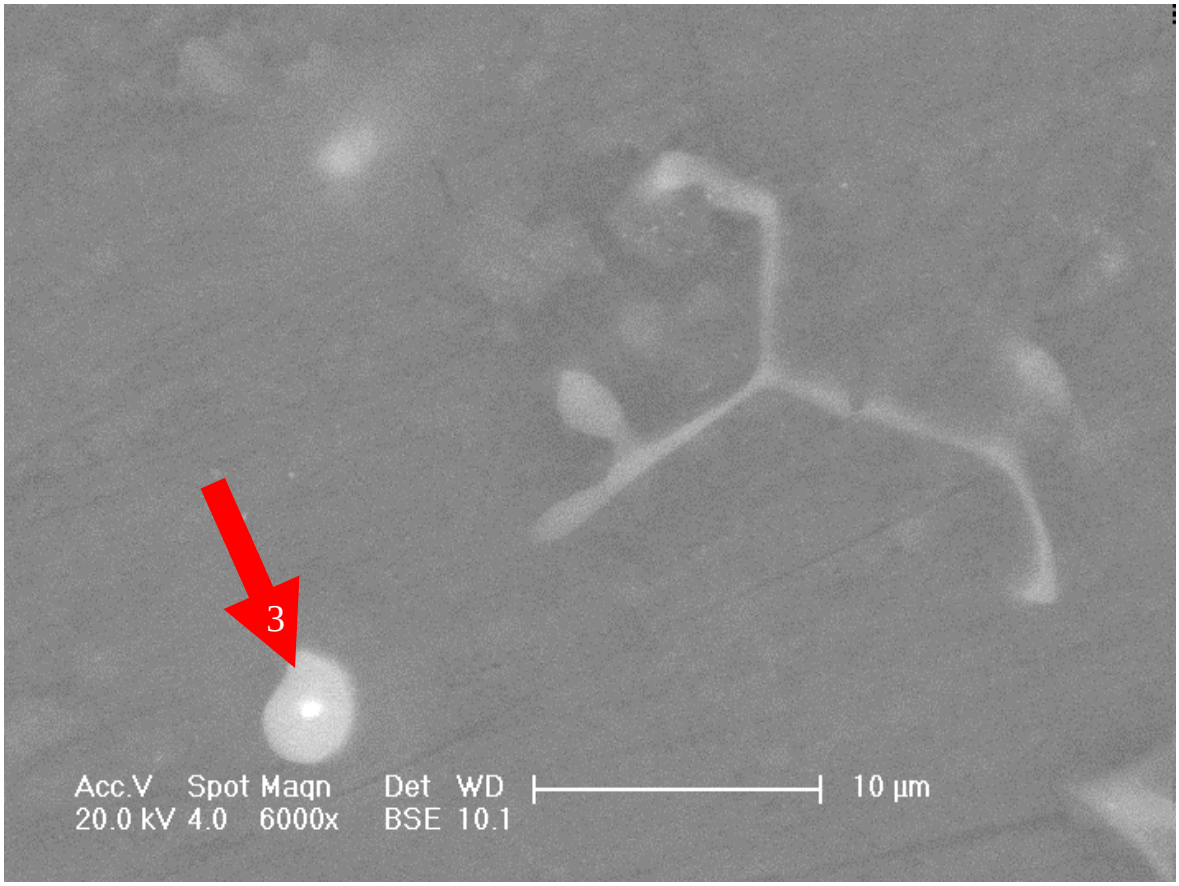

Figure 4.7. A BSE image of the alloy 1

The round phase in Figure 4.7 (mark 3: Alloy 1-3 in Table 4.2) has been investigated with EDS analysis. This phase has a moderate light color with a white spot in the center of the particle and is composed of Mg, Al, Si, and Ca. The light contrast of this phase comes from the Al and Ca concentration. Moreover, the white spot at the center of this phase can be the result of a high Ca concentration. The phase has enveloped the Ca particle within the phase perhaps via a divorced eutectic growth. The amount of Mg, Al, and Ca containing phases are determined using the BSE images is 1,8 area per cent which is the lowest among the four alloying compositions.

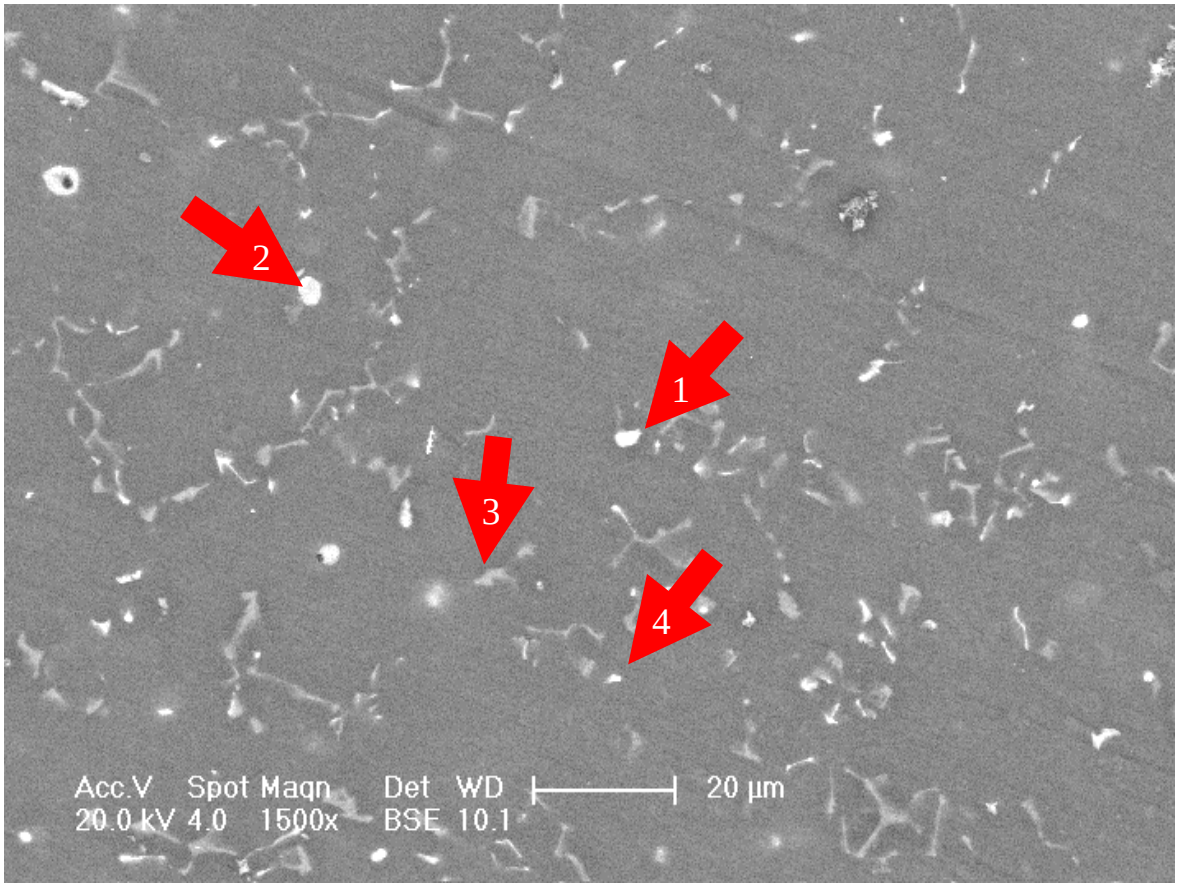

Figure 4.8. A BSE image of the alloy 2

In the alloy 2, blocky particles can be observed in the BSE analyses with different contrasts. In order to investigate the composition of these phases, an EDS analysis has been conducted on them that are marked 1, 2, 3, and 4 in Figure 4.8. The blocky phase (mark 1: Alloy 2-1 in Table 4.2) is composed of Mg, Al, Si, and Ca. The light contrast of this phase comes from high Ca concentration (11,64 weight per cent). The diameter of the beam is larger than the phase's diameter. That's why the surrounding Si atoms in the matrix are added to the results obtained from the EDS analysis. The second phase (mark 2: Alloy 2-2 in Table 4.2) is darker with a bright rim around the phase. This phase is composed of Mg, Al, and Ca. The rim around this phase should be composed of Ca. The lighter contrast of this phase comes from high Al concentration (24,8 weight per cent). This phase is possibly β-$Mg_{17}Al_{12}$. The third phase (mark 3: Alloy 2-3 in Table 4.2) is also composed of Mg, Al, Si, and Ca. It has a Si concentration of 23,08 weight per cent which gives its dark contrast. This is Mg_2Si phase with a coarse blocky morphology. Ca and Al content found within this

phase come from the surrounding matrix. The fourth blocky phase (mark 4: Alloy 2-4 in Table 4.2) for this alloy has a lighter shade and can be seen in Figure 4.8. The whiteness of this phase comes from the high Al concentration (25,61 weight per cent). Since this phase contains only Mg and Al, it should be the β-$Mg_{17}Al_{12.}$ This phase is also located near a Chinese script like feature. The amount of Mg, Al, and Ca containing phases in the alloy 2 is 2 area per cent.

In the alloy 3, the Chinese script like phases and the short rod like features dispersed around these phases can be seen in Figure 4.9. The characteristics of these phases are basically the higher concentrations of Si which gives them their dark color.

An EDS analysis has been conducted on the phases that are marked 1 and 2 in Figure 4.9. The first phase (mark 1: Alloy 3-1 in Table 4.2) contains Mg, Al, Si, and Ca and has a dark color which is a result of high Si concentration (15,22 weight per cent) with low Al and Ca concentrations. The reason for the Al and Ca found in the composition in this analysis is the beam diameter. As the beam diameter is 5 μm and the thickness of the arm of the Chinese script is 1 μm, these elements are read from the periphery of the phase. The phase, again due to its dark color, is thought to correspond to Mg_2Si phase.

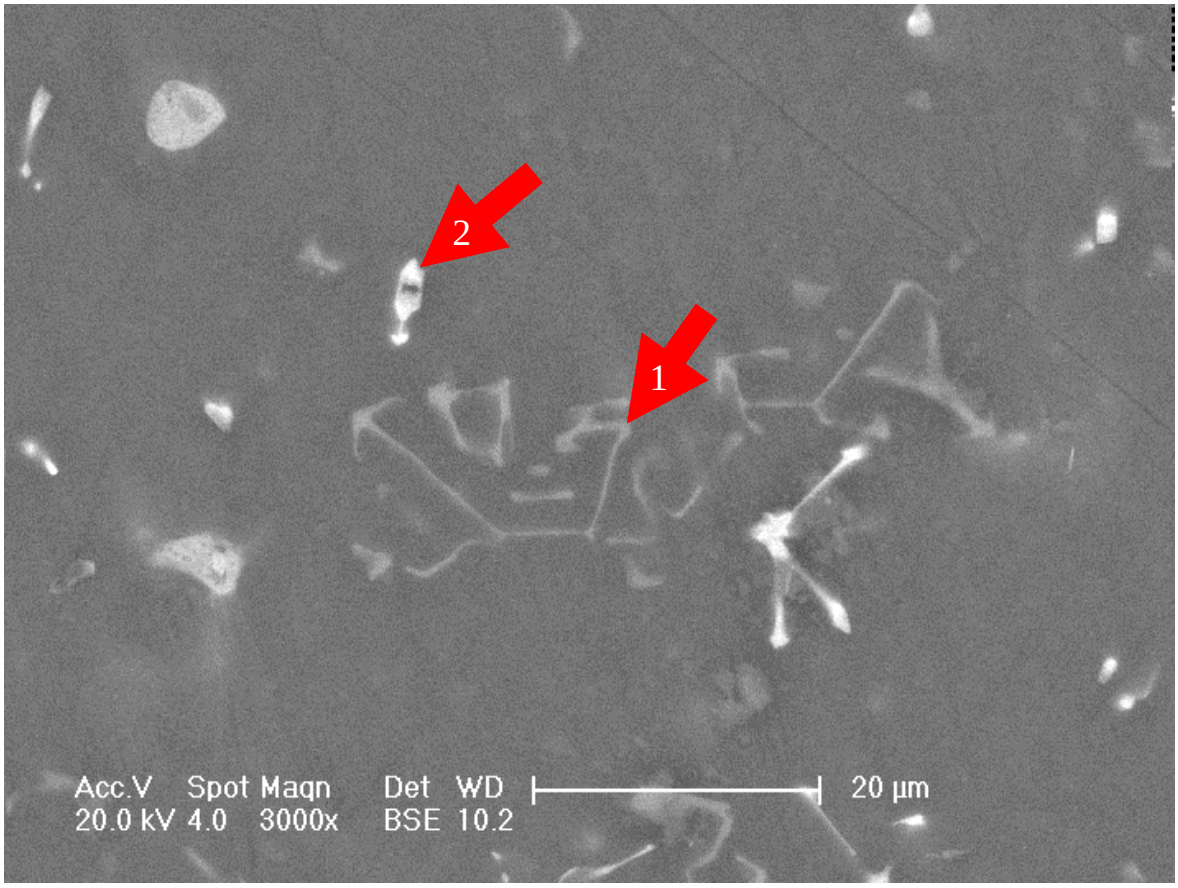

Figure 4.9. A BSE image of the alloy 3

The second phase (mark 2: Alloy 3-2 in Table 4.2) which is a blocky particle has a lighter contrast. Also, it has moderate Si (3,56 weight per cent) and high Al (27,56 weight per cent) concentrations with low Ca concentration (0,26 weight per cent). The dark spot in the center of this phase can be the result of the Si content. The amount of Mg, Al, and Ca containing phases in the alloy 3 is 2,1 area per cent.

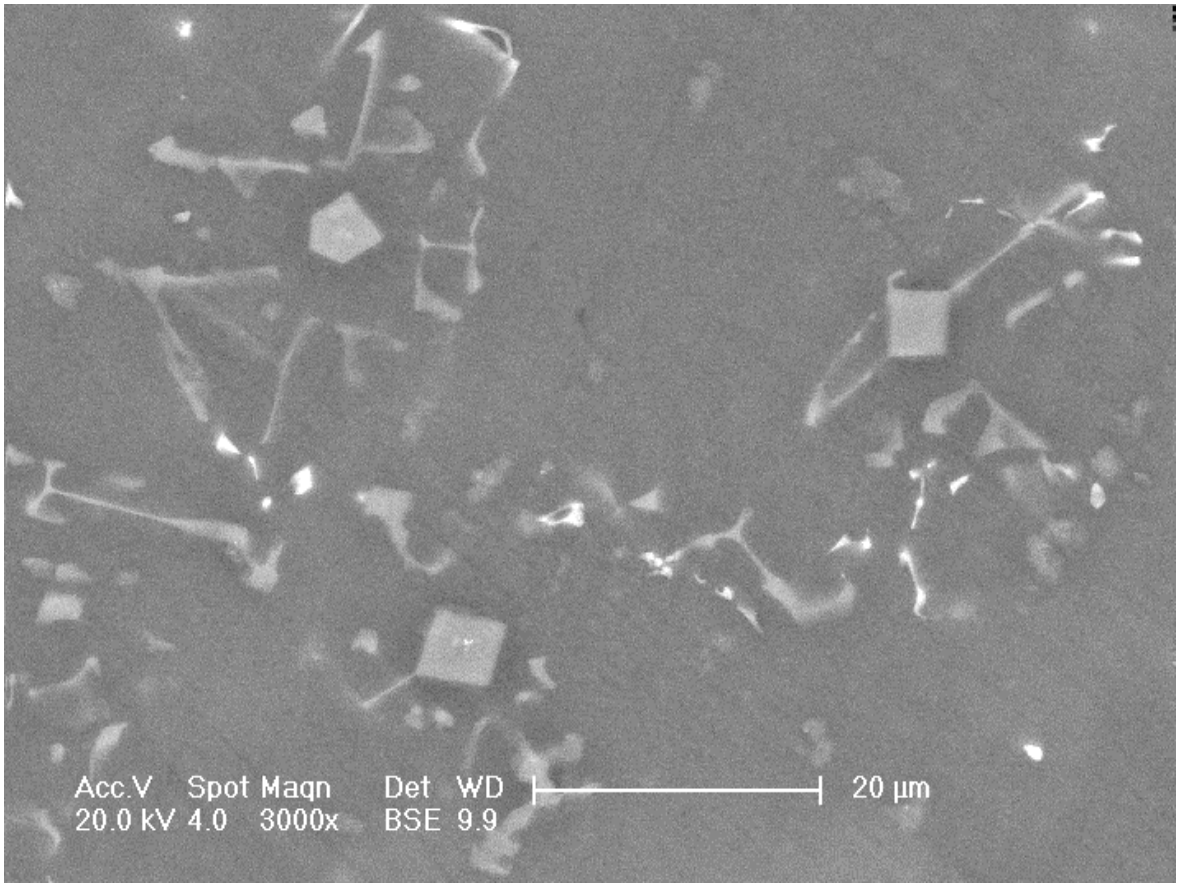

Figure 4.10. A BSE image of the alloy 4

In the alloy 4, short rods emerging from diamond shaped particles can be seen in the BSE analysis. Figure 4.10 shows a detailed image of the morphology of this phase. The increase of Ca within the microstructure of the alloys has led to the formation of the diamond like morphologies. Flat surfaces are an indication of faceted morphology as they are not a result of crystal structure match since Mg_2Si is in the FCC where as Mg matrix is in the HCP structure. In order to investigate the composition of these phases an EDS analyses has been conducted on the short rods and the diamond shaped particles that are marked 1, 2, 3, 4, and 5 in Figure 4.11.

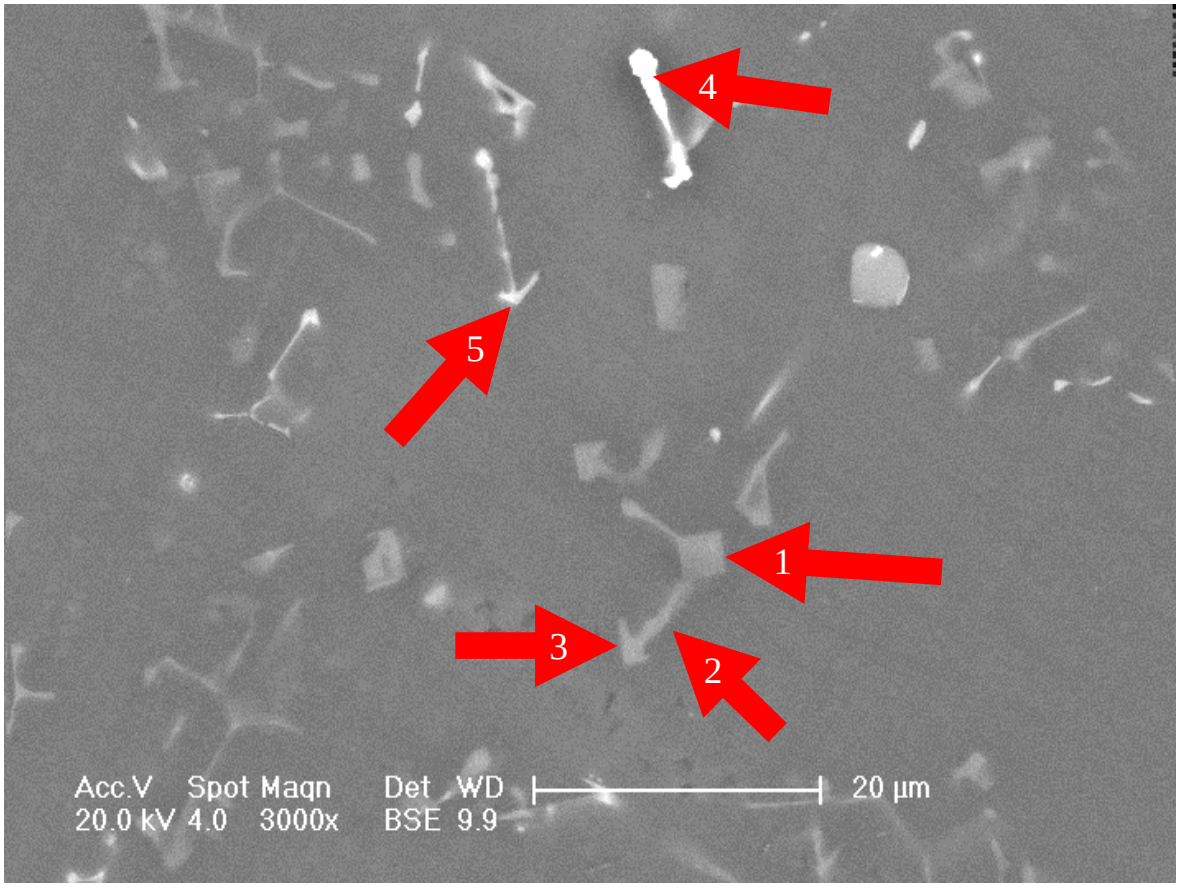

Figure 4.11. A BSE image of the alloy 4

The diamond shaped phase (mark 1: Alloy 4-1 in Table 4.2) is composed of Mg, Al, and Si. The Al content is very low, and Si content is high (19,13 weight per cent) which gives the particle its dark color. The beam diameter is comparable to the size of this diamond shaped particle. The location of the second mark (mark 2: Alloy 4-2 in Table 4.2) is composed of Mg, Al, Si, and Ca with a lower Si (13,92 weight per cent) content. Al and Ca are read because of the wider beam diameter than the size of the short rod. The blocky particle (mark 3: Alloy 4-3 in Table 4.2) at the end of the short rod has a higher Si content (16,58 weight per cent). These spots all conform to Mg_2Si phase composition. The fourth phase (mark 4: Alloy 4-4 in Table 4.2) is composed of Mg and Al. This straight rod shaped phase has a white color. The whiteness of this phase comes from its high Al content (22,9 weight per cent). This phase should be the β-$Mg_{17}Al_{12}$ phase. A similar straight rod phase (mark 5: Alloy 4-5 in Table 4.2) is composed of Mg, Al, Si, and Ca. The high Ca concentration (7,21 weight per cent) of this phase gives its lighter contrast compared to

Mg_2Si. It should be noticed in Figure 4.11 that the short rods mostly ends with an arrow like feature. Amount of the Mg, Al, and Ca containing phases has increased to 2,3 area per cent, which is the highest among the four alloying compositions.

The microphotographs of the specimens analyzed within this thesis work show that blocky particles are formed within the microstructure of the alloys but no lamellar or dendritic morphologies have been observed. The blocky particles have been found to be Mg_2Si particles. In the Introduction, it has been mentioned that Al_2Ca would form for Ca/Al ratios greater than 0,8; however, particles of Al_2Ca have not been observed. Also, Mg_2Ca has been expected to form for Ca/Al ratios lower than 0,8; however, particles of Mg_2Ca have not been observed either. Although Mg and Ca containing phases have been determined, precise identification of such phases requires utilization of quantitative techniques like WDS (Wavelength Dispersive Spectroscopy). In contrast, the analysis carried out in this work by EDS attached to an SEM is only qualitative.

The compositions were based on the AS21 (2,3 per cent Al -1,13 per cent Si- 0,19 per cent Mn- 0,02 per cent Zn) alloy except for the presence of calcium. That's why the microstructure of the alloys developed within this thesis and AS21 resembles each other with similarity in intermetallic compounds. Naturally, the calcium containing phases are not present in AS21. The microstructure of an experimental AS21 alloy is shown in Figure 4.12.

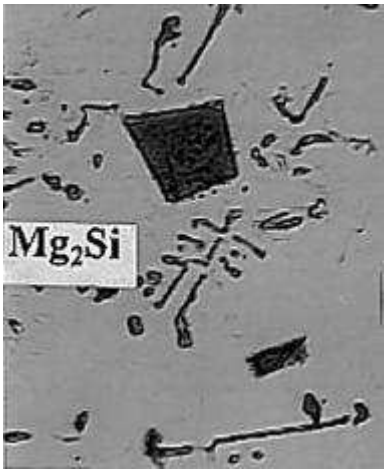

Figure 4.12. Microstructure of AS21 alloy [50]

Observations have shown that AS21 and the alloys developed within this thesis have Mg_2Si phase within the structure, predominantly in Chinese script morphology or in the form of blocky particles with angular outlines. The morphology of these phases is shown in Figure 4.12. Also, AS21 and the alloys developed within this thesis have β-$Mg_{17}Al_{12}$ phase. The main difference in the microstructure lies in the lack of Ca element between the alloys developed and AS21.

Also, the composition of ACM522 (Mg-5 per cent Al-2 per cent Ca-2 per cent M.M-0.3 per cent Mn) alloy is similar to the alloys studied within this thesis except for the presence of silicon in the developed alloys. Therefore, the silicon containing phases are not present in ACM522. The microstructure of an ACM522 alloy is given in Figure 4.13.

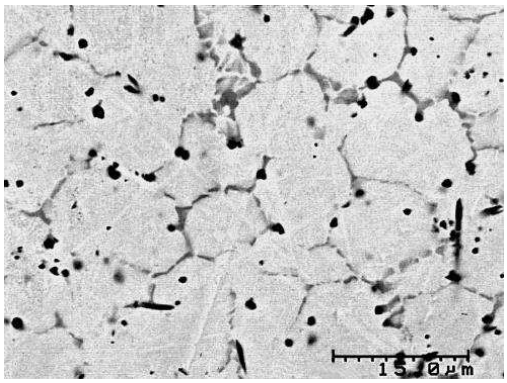

Figure 4.13. Microstructure of ACM522 alloy [23]

Observations have shown that Mg_2Ca, Al_2Ca, and β-$Mg_{17}Al_{12}$ phases are present near the grain boundaries within the ACM522 alloy [23]. In Figure 4.13, Mg_2Ca and Al_2Ca are dispersed around the grain boundaries and have light color. However, only β-$Mg_{17}Al_{12}$ phase have been observed in the alloys developed within this thesis.

One other concept affecting the mechanical properties of the alloy is the porosity of the material. Various levels of porosity have been observed within the microstructure of the developed alloys. The porosity values on the samples have a diminishing effect on the load bearing and impact performance of the alloys. Entrapped gases, solidification shrinkage, or non uniform feeding of liquid during solidification should have resulted in

porosity [57]. The high levels of porosity values should be responsible for the low strength, elongation, and toughness. The porosities of the alloys are given in Table 4.1.

The typical porosity values for other magnesium alloys were given in section 1.1.8. When compared, even the alloy containing the least amount of porosity (alloy 1), has 50 per cent more porosity than the alloys given in section 1.1.8. This should bring a high amount of reduction in the mechanical properties of the alloys.

4.2. Tensile Testing

Mechanical property test results are shown in Table 4.3. Each datum for a particular alloy and test condition is the mean value based on duplicate tests. The microstructural analysis as discussed in the previous section has given useful information on the role of microstructural features on strength, ductility, and other mechanical properties.

The grain size of the alloys, as stated before varies between 5 and 10 μm. Though the Ca content differs between the alloys, the grain size of the alloys is similar. That's why the grain size effect on the mechanical properties has not been discussed here.

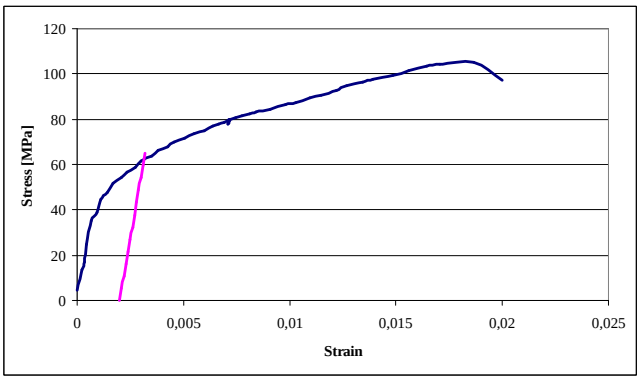

Figure 4.14. Tension curve for the alloy 4, specimen 3 with velocity 10 mm/min. The 0,2 per cent offset line is also shown

Figure 4.14 shows a representative stress and strain diagram for the tested alloys. For all the alloying compositions, the stress-strain variation follows a similar pattern. With the application of tensile loading on the specimen, the alloy first deforms elastically. Once the

yield point has been reached, the plastic deformation starts. The stress increases till the stress-strain diagram reaches the UTS, after which the stress decreases till the fracture.

Table 4.3. Mechanical properties of the tensile specimens

Alloy #	**Pulling Velocity [mm / min]**	**E (GPa)**	**σ_y (MPa)**	**UTS (MPa)**	**Fracture Strength (MPa)**	**Elongation @ Fracture (per cent)**	**n**	**m**	**Toughness [J]**
1	**1**	21,00 ±33	61,75 ±8	112,99 ±14	107,80 ±16	3,65 ±25	0,58 ±12	-0,1 ±20	2,66 ±24
	10	26,00 ±4	49,50 ±1	101,90 ±8	100,00 ±8	2,80 ±9	0,55 ±4		1,98 ±35
2	**1**	32,60 ±4	44,00 ±7	65,51 ±10	41,59 ±32	1,54 ±47	0,50 ±13	0,08 ±37	0,75 ±50
	10	27,50 ±34	52,88 ±4	108,83 ±20	103,64 ±23	2,74 ±18	0,55 ±15		2,12 ±23
3	**1**	19,00 ±47	62,66 ±10	108,31 ±11	96,12 ±4	3,06 ±6	0,54 ±8	0,02 ±33	2,19 ±42
	10	24,50 ±18	66,20 ±5	105,71 ±2	103,47 ±4	1,79 ±44	0,45 ±4		1,46 ±30
4	**1**	43,50 ±1	70,50 ±4	103,81 ±1	101,00 ±2	1,38 ±7	0,34 ±3	-0,02 ±100	1,85 ±36
	10	45,00 ±20	68 ±3	95,84 ±10	95,00 ±10	2,00 ±6	0,41 ±25		1,91 ±10

*The values given in paranthesis are the per cent deviation from the average values shown

The Mg_2Si phases that are present within the alloys especially increase the strength by interconnecting the grains to each other. The strength of these connections increases as the eutectic phases become thicker with increasing amount of calcium, since the increase in the thickness increases the load carrying capacity of the phases. As a matter of fact, the dimensions of Mg_2Si are different in each of the alloying compositions. The arms of the Mg_2Si Chinese script phases have a thickness of 1 μm for the alloys 1 and 2, 2 μm for the alloy 3, and 2-3 μm for the alloy 4. Also, the Mg_2Si blocky particles have a size of 4-5 μm in the alloys 1 and 2, 4 μm in the alloy 3, and 5-8 μm in the alloy 4.

Other phases can also contribute to the mechanical properties. As a matter of fact, β-$Mg_{17}Al_{12}$ is also present in the alloy. Because there is a large spacing between the atoms of β-$Mg_{17}Al_{12}$ phase to have a dispersoid-strengthening effect, this phase has no effect on the elastic deformation of the alloy. However, after elastic deformation, strong interfacial stresses form because of the difference in strength between the ductile α phase and the brittle β-$Mg_{17}Al_{12}$ phase which gives rise to work hardening. However, due to inherent brittleness of this phase, alloys containing this phase also become brittle [57.]. A more detailed investigation on the mechanical properties resulting from the microstructure is given below.

Tensile testing results plotted in Figure 4.15 show that the yield strength has an increasing trend in both of the pulling velocities. For the 1 mm/min pulling velocity, the increase in the yield strength from the alloy 1 (0,7 weight per cent Ca) to the alloy 4 (2 weight per cent Ca) is 12 per cent. For the 10 mm/min pulling velocity, increase in the yield strength from the alloy 1 to the alloy 4 is 27 per cent. The increase of the yield strength is related to the size and morphology of the particles present within the alloys. Small sized particles with enough number and scattered within the matrix, effectively impede the dislocation motion. As a result, the materials having small sized particles have higher yield strength. As a brief note, the dislocations can be introduced during solidification or as a consequence of thermal stresses that result from rapid cooling. Also, specifically the rod like or Chinese script Mg_2Si particles increase the yield strength by interconnecting neighboring grains. As the amount of the Mg_2Si phases increases, the resistance to dislocation motion within the structure increases so that the yield strength of the alloys increases. For instance, the alloy 4 has the highest amount (6,25 area per cent) of the Mg_2Si phase present in the microstructure hence it has the highest yield strength. The abnormal decrease in the yield strength of the alloy 2 pulled with 1 mm/min is related to the blocky particles present within the alloy. These blocky particles are observed to be ineffective in resisting the dislocation motion, perhaps due to their very small sizes and inadequate number.

Furthermore, it is known that materials having positive strain-rate sensitivity have higher yield strength in high pulling velocities when compared to low pulling velocities. The opposite is true for materials exhibiting negative strain-rate sensitivity. In positive

strain-rate sensitive materials, dislocations easily slip in low pulling velocities. In contrast, in high pulling velocities, dislocations lock, preventing further dislocation motion. That's why the yield strength increases with increasing pulling velocities.

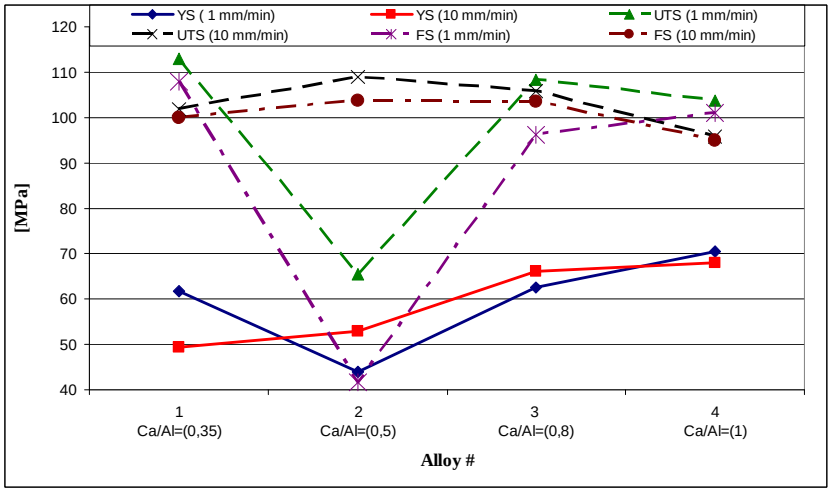

Figure 4.15. Mechanical properties of the alloying compositions

Moreover, Figure 4.15 shows that the UTS has a decreasing trend in both of the pulling velocities. For the 1 mm/min pulling velocity, the decrease in the UTS from the alloy 1 to the alloy 4 is 8 per cent. For the 10 mm/min pulling velocity, the decrease in the UTS from the alloy 1 to the alloy 4 is 6 per cent. This decrease is not significant. Thus it can be stated that the increase in Ca content is ineffective to change the UTS. The UTS is related to the size and morphology of the phases present within the alloys because these features can reduce the mobility of dislocations. The particles that are on the slip planes and in the directions of the dislocations can effectively resist the dislocation motion. Also, as dislocations move, they can pile-up before the particles. Large sized particles can resist a greater pile-up of dislocations than the small sized particles. That's why large sized particles can increase the UTS efficiently. Especially, Mg_2Si particles form connections between the neighboring grains which effectively resist the dislocation motion. Furthermore, the strain hardening exponent increases with increasing resistance to dislocation motion. Thus, the alloys having higher strain hardening exponent have a higher UTS as shown in Table 4.3. The abnormal decrease in the UTS of the alloy 2 is related to the presence of fine blocky particles within the material. These blocky particles cannot effectively resist the dislocation motion after the yield as compared to particles with

Chinese script or large diamond shaped morphology present in the alloy 1, 3, and 4. As a last comment, the slight decrease in the UTS should be related to the increasing porosity values within the alloys. That's why the alloys containing high porosity values have lower UTS.

Also, Figure 4.15 shows that fracture strength has a trend similar to UTS in both of the pulling velocities. For the 1 mm/min pulling velocity, the decrease in the fracture strength from the alloy 1 to the alloy 4 is 6 per cent. For the 10 mm/min pulling velocity, the decrease in the fracture strength from the alloy 1 to the alloy 4 is 5 per cent. Fracture strength is related to the amount of porosity as well as the size and morphology of the phases present within the alloys. The specimens having higher porosity have lower cross-sections which decreases fracture strength. Also, the porosity is a detriment to fracture strength because an applied stress may be amplified at these defects. Thus cracks can form and propagate more easily. That's why the specimens having higher porosity values have lower fracture strength. In contrast, Mg_2Si phases that are present within the alloys increase fracture strength by increasing the resistance to crack formation. Hence, an increase in the amount of Mg_2Si phases is expected to increase the fracture strength. However, once the cracks form due to porosity, Mg_2Si phases cannot resist crack propagation especially because of the slenderness of the Chinese script morphology. Thus, the slight decrease in fracture strength should be related to the increasing porosity values as well as to the thin fibers of the Mg_2Si Chinese script phase within the alloys. The abnormal decrease in the alloy 2 is related to the high porosity values present within the alloy and ineffective resistance of the small blocky particles to crack formation as these phases have a lower stiffness than Mg_2Si phases.

In the next figure, Figure 4.16, it is shown that Young's modulus has an increasing trend in both of the pulling velocities. The magnitude of the Young's modulus is a measure of the resistance to separation of adjacent atoms. The increase in the Ca content is observed to increase the resistance of the atoms to separation for both pulling velocities. That's why it is claimed that increasing the Ca content increases the Young's modulus (E). The slight decrease of the Young's modulus in the alloy 2 should be related to the weaker bonds formed for this composition.

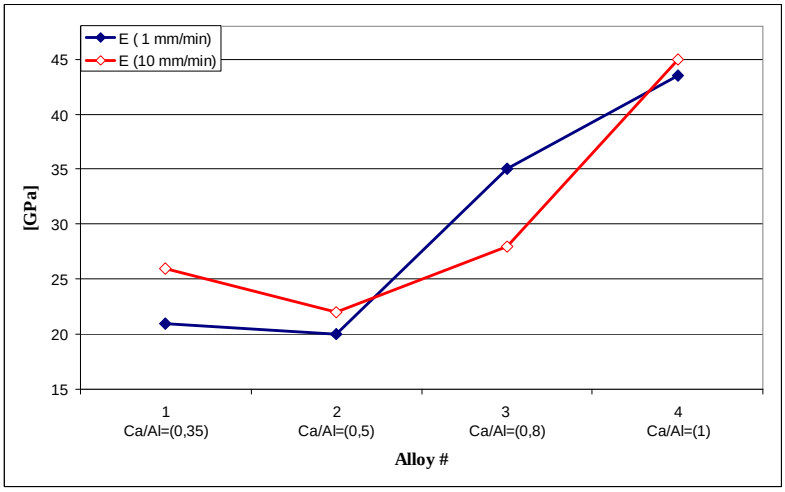

Figure 4.16. Young's modulus of the alloying compositions

The strain hardening exponent is plotted in Figure 4.17. It's seen that strain hardening exponent has a decreasing trend with increased Ca content in both of the pulling velocities. The decrease in the strain hardening exponent is related to the increase in the mobility of dislocations within the structure, as explained before. Also, the decrease in the strain hardening exponent decreases ε_t (true strain) as the magnitude of these properties is equal at the UTS. This results in a decrease in the material's uniform deformability before the onset of necking. That's why the specimen's having lower strain hardening exponent values will be fractured at lower strains.

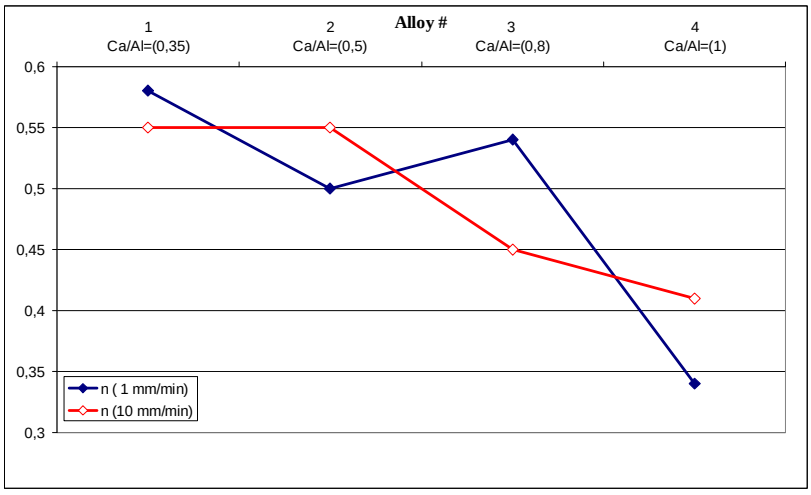

Figure 4.17. Strain-hardening exponent values of the alloying compositions

Next, Figure 4.18 shows that strain-rate sensitivity (m) has a decreasing trend from the alloy 2 to the alloy 4. The decrease of the strain-rate sensitivity can be related to the morphology and amount of phases present within the alloys. The Mg_2Si particles with Chinese script morphology are observed to ineffectively impede dislocation motion in high pulling velocities in contrast to blocky particles. As a result, the strain hardening exponent decreases with increasing Ca content. The anomaly for the alloy 1 should be related to the low amount of Chinese script phases present within the alloy. The low amount of Chinese script particles cannot impede dislocation motion effectively at a high pulling velocity. Also, brittle phases break easier with impact (high velocity) loading.

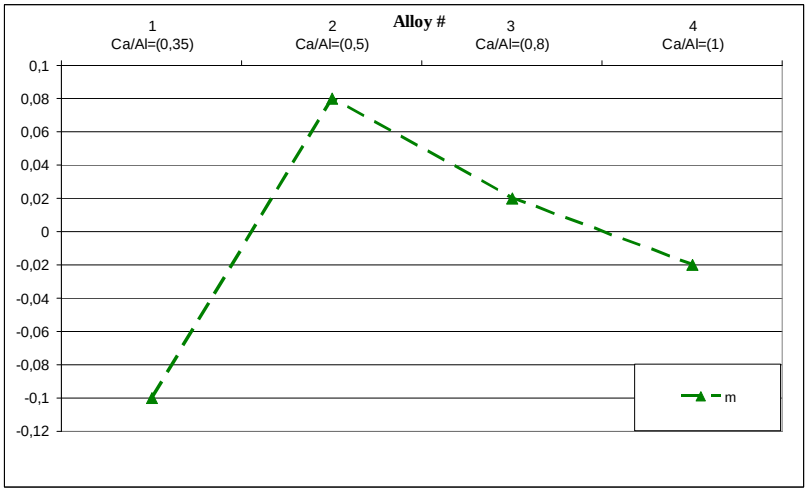

Figure 4.18. Strain-rate sensitivity values of the alloying compositions

It's shown in Figure 4.19 that toughness has a decreasing trend with an anomaly for the alloy 2 for 1 mm/min pulling velocity. For the 1 mm/min pulling velocity, the decrease in the toughness from the alloy 1 to the alloy 4 is 30 per cent. For the 10 mm/min pulling velocity, the decrease in the toughness from the alloy 1 to the alloy 4 is 4 per cent. The increase in the Ca content increases the brittleness of the alloys. This results in the decrease of the toughness of the material. The anomaly for the alloy 2 for the pulling velocity of 1 mm/min is related to the presence of the blocky particles. These particles decrease the toughness of the alloy by decreasing the yield strength and the UTS by ineffectively resisting the dislocation motion.

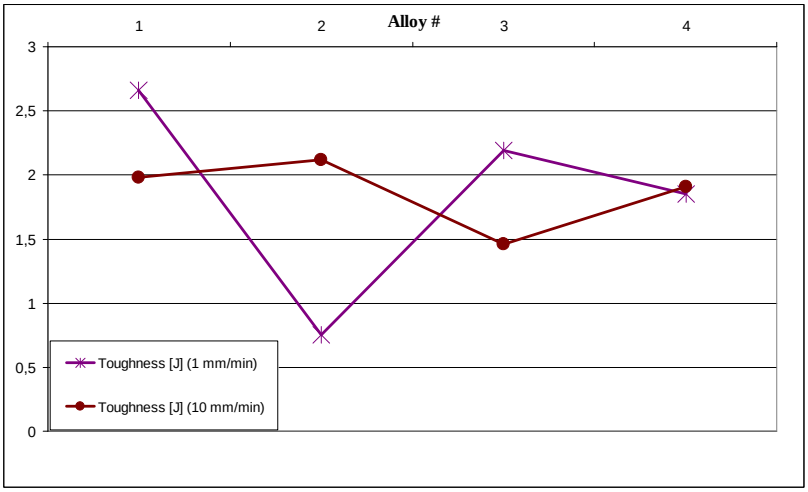

Figure 4.19. Toughness values of the alloying compositions

Lastly, the elongation values are shown in Figure 4.20. Elongation follows a decreasing trend as the Ca content increases. For the 1 mm/min pulling velocity, the decrease in the elongation from the alloy 1 to the alloy 4 is 60 per cent. For the 10 mm/min pulling velocity, the decrease in the elongation from the alloy 1 to the alloy 4 is 28 per cent. It's therefore proposed once more that the increase in the Ca content of the alloy increases the brittleness.

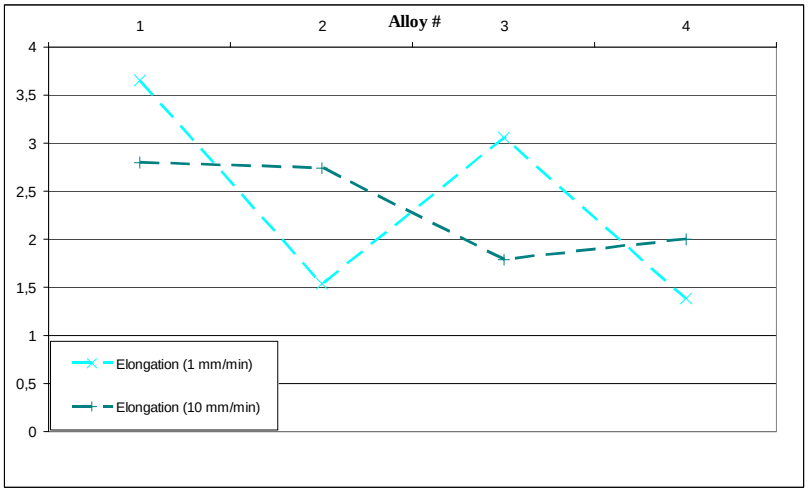

Figure 4.20. Elongation values of the alloying compositions

The mechanical properties should be compared with similar alloys in order to interpret the observations of the current research. ACM522, AS21, and an alloy (hereafter called BU alloy) developed in Boğaziçi University with the chemical composition Mg-Al-Si-Mn-Ca (95,95 per cent Mg-1,9 per cent Al -1,1 per cent Si- 0,4 per cent Mn- 0,65 per cent Ca) have similar alloying compositions. The mechanical properties of these alloying compositions are given in Table 4.4.

Table 4.4. Properties of ACM522 [23], AS21 [50], BU Alloy [59], and Alloy #4

Mechanical property	**ACM522**	**AS21**	**BU Alloy**	**Alloy #4**
Compressive Yield Strength [MPa]	140	120	111	70,50
Tensile Yield Strength [MPa]	140	120	-	70,50
UTS [MPa]	200	220	-	103,8
Young's Modulus [GPa]	45	45	45	43,5
Elongation at Fracture [per cent]	3	9	13	1,38

According to the mechanical testing results of the alloys developed within this thesis, the highest mechanical properties belong to the alloy number four. The other alloys have significantly (25-50 per cent) lower values. The mechanical properties of the alloy 4 will be compared with the other three alloying compositions given in Table 4.4.

ACM522 is a high-pressure-die-cast alloy having nearly zero porosity. It has the highest compressive and tensile yield strength among the alloys given in Table 4.4. This does imply that the alloy 4 may have higher strength with zero porosity. Moreover, the Mg_2Ca and Al_2Ca phases may have contributed to the high strength values in ACM522. Also, ACM522 shows a low elongation value which is similar to the alloy 4 which confirms the incremental affect of Ca on brittleness. Young's modulus is similar for each of the alloying compositions because the matrix and interatomic forces of these alloys are similar.

AS21 is also a high-pressure-die-cast alloy having nearly zero porosity. The tensile and compressive strength values of the AS21 are second among the given 4 alloys.

However, it has higher elongation values. Thus the removal of Ca from the alloy composition lowers the strength but increases the elongation values.

BU alloy is a permanent-mold cast alloy, which has a very similar alloying composition with the alloy 4. This alloy exhibits the third highest compressive yield strength. However, this composition still shows higher compressive yield strength values than the alloy 4, even though the microstructural features of both of the alloys are similar. Both of the alloys have exhibited Mg_2Si with Chinese script morphology and polyhedral, blocky particles. Also, the BU alloy has distinct phases with lamellar, feathery and whisker like morphologies [59]. As the porosity values and the phase amount for BU alloy have not been investigated, the reasons for the difference between BU alloy and the alloy 4 can not be ensured. However, about 40 per cent decrease in compressive strength in the alloy 4 should be due to the presence of Ca.

It is worth mentioning that ACM522 and AS21 alloys can provide higher mechanical properties then alloy 4, but these high values are not necessary for oil pans. As a brief note, the maximum stresses occurring on the oil pan is between 60 and 70 MPa and the strain is 0,7 per cent. That’s why it can be suggested that the alloy 4 has the necessary mechanical properties for oil pans.

Lastly, the alloy 4 has significantly increased the mechanical properties of pure magnesium which is shown in Table 1.2.

4.3. Compression Testing

Mechanical properties of the four alloys have been investigated using 8 specimens with two compression velocities. The results seen in Table 4.5 are the mean values based on duplicate tests.

Table 4.5. Mechanical properties of the compression specimens

Alloy #	**1**	**2**	**3**	**4**
σ_y (MPa)	61	65	68	76
E (GPa)	21	29	24	38

Figure 4.21 shows a representative stress and strain diagram for compression testing for the developed alloy. For all the alloying compositions, the stress variation follows a similar pattern. With the application of compressive loading on the specimen, the alloy first deforms elastically. Once the yield point has been reached, the plastic deformation starts.

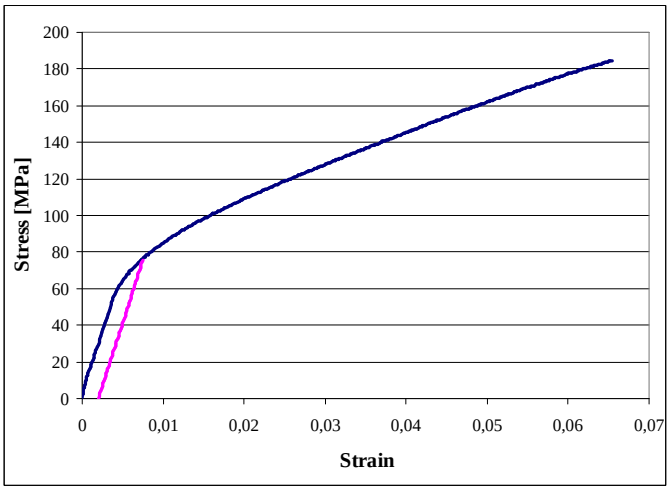

Figure 4.21. Compression curve for alloy 3 with the offset line

From the results of compression testing, it can be observed that the compressive yield strength of the material increases with the increased Ca content in the composition of the specimen. There is an increase of 20 per cent in the yield strength of the material from the alloy 1 to the alloy 4. Moreover, the formation of the Mg_2Si phases increases the yield strength of the material. The increase of the yield strength is similar to that in tensile case as the particles present within the alloy impedes the dislocation motion in tension and compression in a similar way. Nevertheless, the reason for low E values in compression requires a further investigation.

Comparison of tensile data in Table 4.3 and compressive data in Table 4.5 shows that strength values are not far apart. In fact, slight variations may be attributed to the hexagonal crystal structure. It's well known that, due to the limited number of slip systems in HCP's, twinning is a common deformation mode. Twinning deformation mode in a crystallite is activated only if it is oriented in a specific way with respect to the loading. This may lead to tension compression anisotropy in materials.

4.4. CAE Analysis

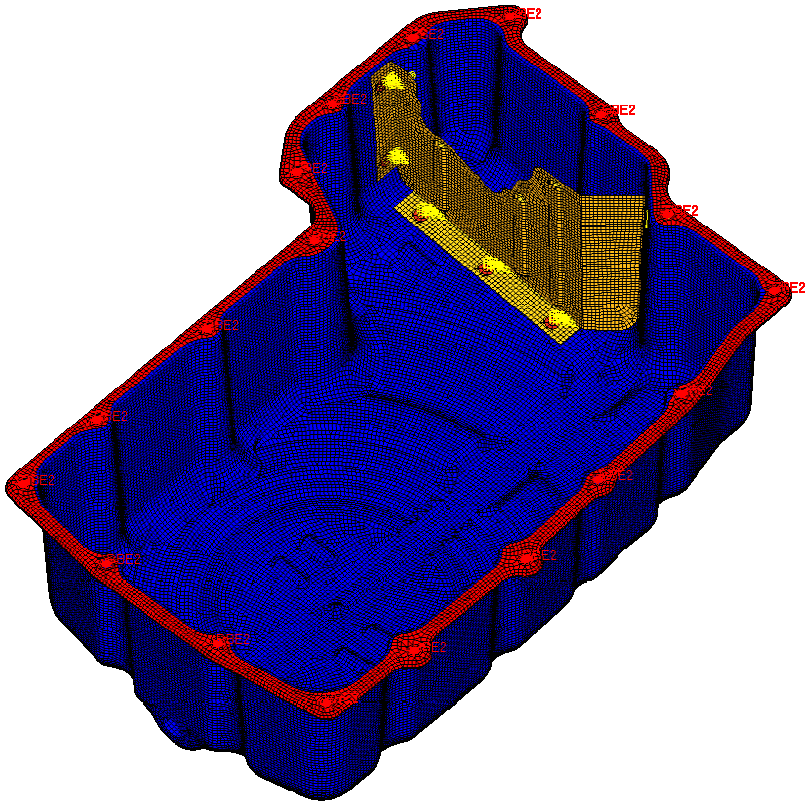

Figure 4.22. Magnesium I5-Oil Pan

The models of the currently used steel oil pan and the newly developed magnesium alloy oil pan have been developed, and the normal modes analysis has been conducted. The meshed model of the oil pan is shown in Figure 4.22. Representative results can be seen in Figure 4.23. The mode shape on the top is for steel oil pan and the bottom is for magnesium oil pan

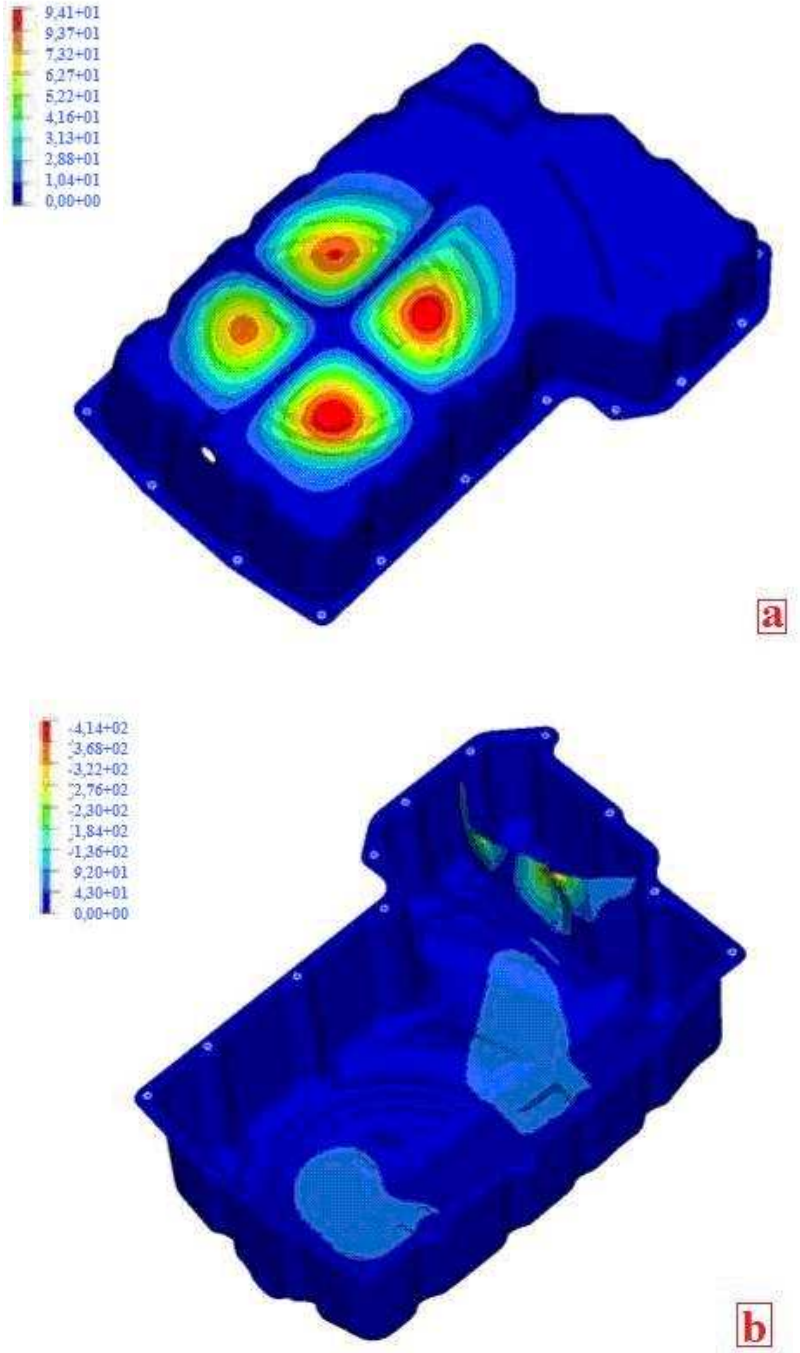

Figure 4.23. Mode shapes: (a) Steel oil pan mode 6 and (b) Magnesium oil pan mode 6

Table 4.6. Natural frequencies of steel and magnesium oil pan

Modes	Steel Oilpan [Hz]	Magnesium Oil Pan [Hz]	Modes	Steel Oilpan [Hz]	Magnesium Oil Pan [Hz]
1	2,94E+02	3,09E+02	**24**	1,30E+03	1,85E+03
2	3,62E+02	5,45E+02	**25**	1,31E+03	1,95E+03
3	4,84E+02	5,78E+02	**26**	1,35E+03	2,01E+03
4	5,28E+02	8,98E+02	**27**	1,38E+03	2,04E+03
5	6,38E+02	9,29E+02	**28**	1,40E+03	2,06E+03
6	7,03E+02	9,64E+02	**29**	1,42E+03	2,09E+03
7	7,55E+02	1,06E+03	**30**	1,44E+03	2,11E+03
8	7,90E+02	1,16E+03	**31**	1,49E+03	2,15E+03
9	8,15E+02	1,23E+03	**32**	1,50E+03	2,19E+03
10	8,46E+02	1,29E+03	**33**	1,51E+03	2,23E+03
11	9,18E+02	1,36E+03	**34**	1,52E+03	2,28E+03
12	9,87E+02	1,39E+03	**35**	1,59E+03	2,30E+03
13	1,00E+03	1,46E+03	**36**	1,59E+03	2,35E+03
14	1,01E+03	1,51E+03	**37**	1,61E+03	2,41E+03
15	1,04E+03	1,62E+03	**38**	1,63E+03	2,43E+03
16	1,06E+03	1,63E+03	**39**	1,70E+03	2,49E+03
17	1,06E+03	1,64E+03	**40**	1,71E+03	2,53E+03
18	1,07E+03	1,69E+03	**41**	1,73E+03	2,59E+03
19	1,12E+03	1,71E+03	**42**	1,76E+03	2,61E+03
20	1,15E+03	1,74E+03	**43**	1,78E+03	2,68E+03
21	1,21E+03	1,80E+03	**44**	1,80E+03	2,68E+03
22	1,23E+03	1,84E+03	**45**	1,81E+03	2,69E+03
23	1,28E+03	1,86E+03			

Magnesium oil pan tolerates higher natural frequencies in each mode. This gives an advantage to the magnesium oil pan as lower frequencies are more dominant in the engines and magnesium oil pan will have less resonance occurring in the engine running conditions. Also, the weight of the oil pans has been calculated. The magnesium oil pan provides a 45 per cent weight reduction from the current oil pan.

5. CONCLUSIONS

In today's world, decreasing the weight of vehicles has utmost importance. One of the ways of decreasing the weight of vehicle is by reducing the weight of its parts by using lighter materials. The engine of a car is one area to gain high weight decrease with the usage of lighter materials. Within this study a new magnesium alloy has been developed which can be used for light duty truck oil pans attached to the engine.

Four magnesium alloys with different compositions have been developed. These alloys have different calcium concentrations. The tensile and compressive properties of these alloys have been investigated by means of microstructural analysis and mechanical testing.

The microstructural analysis has shown that the specimens which have higher calcium concentration have high strength but low ductility. This results from the variation of the amount and morphology of the intermetallic phases. In the alloy 1, connected short rods forming the Chinese script phase morphology have formed. Also, a few blocky particles scattered around these phases have been observed. These short-rod connected Chinese script morphology improves the elongation and toughness of the specimens. In the alloy 2, blocky particles have been formed. These particles have low resistance against dislocation motion. That's why the strength of the alloy 2 is lower. In the alloy 3, the Chinese script phases forms. These phases increase the resistance against dislocation motion. In the alloy 4, the short rods emerging from diamond shaped particles are formed. This phase resists the dislocation motion effectively by pinning the connected phases thus increasing the strength of the material. However, the toughness and elongation of this composition decreases. Also, the blocky particles are observed to be inefficient to resist dislocation motion.

One of the reasons for the low strength of the alloys is the presence of high porosity. With lower porosity levels, the alloys may have higher mechanical properties. Also, another reason is lack of the formation of Mg_2Ca and Al_2Ca phases. These phases can effectively increase the strength of the alloys.

The experiments have shown that the alloy 4 has the necessary mechanical properties to endure the stresses and strains occurring in the oil pan in engine running conditions. Also, ACM522 and AS21 alloys can provide higher mechanical properties but these high values are not necessary for oil pans. That’s why the alloy 4 can be used for the material of the I5 oil pan. As a brief note, the maximum stresses occurring in the oil pan is between 60 and 70 MPa and the strain is 0,7 per cent.

Moreover, lower frequencies are more dominant in the engines and less resonance occurs in lower frequencies in the engine running conditions. Magnesium oil pan has obtained higher natural frequencies than I5 steel oil pan in each mode in CAE analysis. Thus it’s shown that less resonance occurs in magnesium oil pans.

Also, the models have shown that magnesium oil pan provides a 45 per cent weight reduction from the current oil pan which can improve the fuel efficiency of the vehicle.

Lastly, these alloys will provide a cost effective solution for a magnesium alloy that will be used for mass produced light weight oil pans as calcium and silicon are inexpensive elements. That’s why the alloy 4 can be used for light duty truck oil pans as it provides the necessary properties for the part with low weight and cost.

6. SUGGESTED FUTURE WORK

The effect of higher calcium concentration should be studied due to its impact on the toughness and ductility of the alloy.

Mg_2Ca and Al_2Ca phases should be formed to observe the effects of these phases on the mechanical properties of the all

Additionally, the alloy should be cast using a HPDC machine for having lower porosity levels and the mechanical properties of this alloy should be investigated for optimizing the mass production of the alloy for an automotive part.

More precise chemical analysis of phases by WDS and/or TEM should be conducted.

The creep and corrosion testing should be conducted to investigate these properties of the alloys.

7. REFERENCES

1. Rausch, G. and A. Ziese, "Advanced Manufacturing Technology for Automotive Chassis Components through Extensible and Sustainable use of Mg Alloys", *6. International Conference on Magnesium Alloys and Their Applications*, Wolfsburg, November 2003.

2. Mehta, D. S., S. H. Masood, and W. Q. Song, "Investigation of Wear Properties of Magnesium and Aluminum Alloys for Automotive Applications", *Journal of materials processing technology*, Vol. 155-156, pp. 1526-1531, 2004.

3. *Magnesium encyclopedia*, http://www.magnesium.com/w3/data-bank/article.php?mgw=152&magnesium=102, 2009.

4. Avedevisian**,** M.M., *Magnesium and Magnesium Alloys*, ASM International by the Materials Information Society, 1999.

5. Davies, C. and M. Barnett, "Expanding the Extrusion Limits of Wrought Magnesium Alloy"s, *Journal of the Minerals, Metals and Materials Society*, Vol. 56, No. 5, pp. 22-24, 2004.

6. Pekguleryuz, M.O., H. Kaplan, R. Neelameggham, J. Hryn, E. Nyberg, B. Powell, G. Cole, and J.F. Nie, "Magnesium Technology 2002, Part I Primary Production, Environmental Issues, High-Temperature Alloys", *Journal of the Minerals, Metals and Materials Society*, Vol. 54, No. 8, pp. 18-21, 2002.

7. Hollfigl-Rosta, F., E. Just, J. Kohler, and H.J. Melzer, "Magnesium in Volkswagen", Journal of Light Metals Age, Vol. 6, pp. 22-29, 1980.

8. Luo, A. and T. Shinoda, "A New Magnesium Alloy for Automotive Powertrain Applications", *SAE Technical Paper Series*, 980086.

9. Esdaile, R. J., “Magnesium Casting Applications in the Automotive Industry”, *SAE Technical Paper Series*, 2001-01-0415, 2001.

10., Cartner, N., “New Technologies Allow Greater Use of Magnesium”, *TriBology & Lubrication Technology Articles*, Vol. 60, No. 3, pp. 15, 2004.

11. Cole, G., “Magnesium Applications in Ford's PNGV Mondeo”, Procedings *International Magnesium Association 54th World Conference*, pp 24-31, 1997.

12. *Railback*, “Abundance and Form of the most Abundant Elements in Earth’s Ccontinental Crust”, http://www.gly.uga.edu/railsback/FundamentalsIndex.html, 2008.

13. Dargusch, M.S., A.L. Bowles, K. Pettersen, P. Bakke, and G.L. Dunlop, “The Effect of Silicon Content on the Microstructure and Creep Behavior in Die-Cast Magnesium AS Alloys”, *Metallurgical and materials transactions A*, Vol. 35A, pp. 1905-1909, 2004.

14. *International Magnesium Association*, http://www.intlmag.org/statistics. html, 2009.

15. ASM, *Metals Handbook Volume 3 - Alloy Phase Diagrams*, ASM International, 1992.

16. Suzuki, A., N.D. Saddock, J.W. Jones, and T.M. Pollock, “Phase Equilibria in the Mg-Al-Ca Ternary System at 773 and 673 K”, *Metallurgical and Materials Transactions A*, Vol. 37A, pp. 975-983, 2006.

17. Suzuki, A., N.D. Saddock, J.R. Terbush, B.R. Powell, J.W. Jones, and T.M. Pollock, “Precipitation Strengthening of a Mg-Al-Ca–Based AXJ530 Die-cast Alloy”, *Metallurgical and Materials Transactions A*, Volume 39A, pp. 696-702, 2008.

18. Suzuki, A., N.D. Saddock, J.W. Jones, and T.M. Pollock, “Structure and Transition of Eutectic $(Mg,Al)_2Ca$ Laves Phase in a Die-cast Mg–Al–Ca Base Alloy”, *Scripta Materialia*, Vol. 51, No. 10, pp. 1005-1010, 2004.

19. *Automation creation Inc*., www.matweb.com, 2009.

20. Cao, P., and Ma Qian D.H. St. John, "Effect of Iron on Grain Refinement of High-purity Mg–Al Alloys", *Scripta Materialia*, Vol. 51, No. 2, pp. 125-129.

21. Suzuki, A., N.D. Saddock, L. Riester, E. Lara-Curzio, J.W. Jones, and T.M. Pollock, "Effect of Sr Additions on the Microstructure and Strength of a Mg-Al-Ca Ternary Alloy", *Metallurgical and Materials Transactions A*, Vol. 38, No. 2, pp. 420-427, 2007.

22. Rokhlin, L. L. and N. I. Nikitina, "Effect of Calcium on the Properties of The Mg-Al System", *Metal Science and Heat Treatment*, Vol. 45, No. 5-6, pp. 171-173, 2003.

23. Koike, S., K. Washizu, S. Tanaka, T. Baba and K. Kikawa, "Development of Lightweight Oil Pans Made of a Heat-Resistant Magnesium Alloy for Hybrid Engines", *SAE Technical Paper Series*, 2000-01-117.

24. Powell, B. R., A. A. Luo, V. Rezhets, J. J. Bommarito, and B. L.Tiwari, "Development of Creep-Resistant Magnesium Alloys for Powertrain Applications: Part 1 of 2", *SAE Technical Paper Series*, 2001-01-0422.

25. Pekguleryuz, M., P. Labelle and D. Argo, "Magnesium Die Casting Alloy AJ62x with Superior Creep Resistance, Ductility and Die Castability", *SAE Technical Paper Series*, 2003-01-0190.

26. Druschitz, A. P., E. R. Showalter, J. B. McNeill, and D. L. White, "Evaluation of Structural and High-Temperature Magnesium Alloys", *SAE Technical Paper Series*, 2002-01-0080.

27. Berkmortel, J. J. and H. H. J. E. Kearns and J. E. Allison, "Die Castability Assessment of Magnesium Alloys for High Temperature Applications: Part 1 of 2", *SAE Technical Paper Series*, 2000-01-1119.

28. Gertsberg, G., N. Nagar, M. Lautzker, B. Bronfin, N. Moscovitch, and S.Schumann, "Effect of HPDC Parameters on the Performance of Creep Resistant Alloys MRI153M and MRI230D", *SAE Technical Paper Series*, 2005-01-0334.

29. Nyberg, E. A., R. H. Jones, S. G. Pitman, R. D. Carnahan, and R. F. Decker, "High Temperature-Creep Resistant Magnesium Alloys: Advances in Thixomolding Automotive Components", *SAE Technical Paper Series*, 2000-01-1126.

30. Callister, W. D. C., *Materials Science and Engineering: An Introduction*, Wiley International, 2003.

31. Dieter, G. E., *Mechanical Metallurgy*, Mc Graw-Hill Book Co, 1998.

32. Kainer, K.U., *Magnesium: Proceedings of the 6th International Conference Magnesium Alloys and Their Applications*, John Wiley & Sons Inc, 2004.

33. Chadha, G., J. E. Allison, and J. W. Jones, "The Role of Microstructure on Ductility of Die-Cast AM50 and AM60 Magnesium Alloys", *Metallurgical and Materials Transactions A*, Vol. 38A, pp. 286, 2007.

34. Potzies, C. and K. U. Kainer, "Fatigue of Magnesium Alloys", *Advanced Engineering Materials*, Vol. 6, No. 5, pp. 281-289, 2004.

35. Ashby, M. F., *Materials Selection in Mechanical Design*, Butterworth-Heinemann, 2005.

36. LUO, A. A., "Magnesium: Current and Potential Automotive Applications", "*The Minerals, Metals and Materials Society*", *Conference Review*, pp. 42-48, 2002.

37. Tharumarajah, A., and P. Koltun; "CSIRO Manufacturing & Infrastucture Technology, Lifecycle Assessment of Magnesium Component Supply Chain", *IMA World Mg Conference*, 2005.

38. *Honda*, http://automobiles.honda.com/insight-hybrid/specifications.aspx, Honda Motor Company, 2009.

39. ASM, *Metals Handbook Volume 15 - Castings*, ASM International, 2008.

40. Han, L., D. O. Northwood, X. Nie, H. Hu, "The Effect of Cooling Rates on the Refinement of Microstructure and the Nanoscale Indentation Creep Behavior of Mg–Al–Ca Alloy", *Materials Science and Engineering A*, Vol. 512, No. 1-2, pp. 58-66, 2009.

41. ASM, *Metals Handbook Volume 9 - Metallography and Microstructure*, ASM International, 2004.

42. Kunst, M., A. Fischersworring-Bunk, M. A. Gibson, and G. Dunlop, **"**Mechanical Property Evaluation of Permanent-Mould Cast AM-SC1TM Mg-Alloy", *SAE International Journal of Materials and Manufacturing*, Vol. 1, No. 1, pp. 111-121, 2009.

43. Das, S., "Magnesium for Automotive Applications: Primary Production Cost Assessment"*, Journal of the Minerals, Metals and Materials Society*, Vol. 55, No. 11, pp. 22-26, 2003.

44. Clemex Technologies Inc., *Clemex Captive Image Analysis Software*, Version 4.

45. Wayne, R. *IMAGEJ*, version 1,42l, Research Services Branch of the National Mental Institute of Mental Health.

46. ASTM, *E8M – 00b (METRIC) Standard Test Methods for Tension Testing of Metallic Materials*, An American National Standard.

47. ASTM, *E9 – 89a (Reapproved 2000) Standard Test Methods of Compression Testing of Metallic Materials at Room Temperature*, An American National Standard.

48. Altair**,** *Hypermesh*, version 8.0SR1.

49. Kim, J.J., D.H. Kim, K.S. Shin, N.J Kim., "Modification of Mg_2Si morphology in squeeze cast Mg-Al-Zn-Si alloys by Ca or P addition", *Scripta Materialia*, Vol. 41, No. 3, pp. 333-340, 1999.

50. Bronfin, B., M. Katsir, E. Aghion, **"**Preperation and solidification features of AS21 magnesium alloy", *Materials Science and Engineering: A*, Vol. 302, No. 1, pp. 46-50, 2001.

51. Porter, D.E. and K.E. Easterling, *Phase Transformations in Metals and Alloys*, Chapman and Hall Publication, 1990.

52. Suzuki, A., N.D. Saddock, J.W. Jones and T.M. Pollock, "Solidification Paths and Eutectic Intermetallic Phases in Mg–Al–Ca Ternary Alloys", *Acta Materialia*, Vol. 53, No. 9, pp. 2823-2834, 2005.

53. Stefanescu, D. M., *Science and Engineering of Casting Solidification*, Springer, 2002

54. Huheey, J.E., E.A. Keiter, and R.L. Keiter, *In Inorganic Chemistry: Principles of Structure and Reactivity*, 4th edition, HarperCollins, 1993.

55. Luo**,** A A., M. P. BALOGH, and B. R. POWELL, "Creep and Microstructure of Magnesium-Aluminum-Calcium Based Alloys", *Metallurgical and Materials Transactions A*, Vol. 3, No. 3, pp 567-574, 2002.

56. Dargusch, M.S., A.L. Bowles, K. Pettersen, P. Bakke, and G.L. Dunlop, **"**The Effect of Silicon Content on the Microstructure and Creep Behavior in Die-Cast Magnesium AS Alloys", *Metallurgical and Materials Transactions A*, Vol. 35, No. 6, pp 1905-1909, 2004.

57. Huang, Y.J., B.H. Hu, I. Pinwill, W. Zhou and D.M.R. Taplin, "Effects of Process Settings on the Porosity Levels of AM60B Magnesium Die Castings"**,** *Materials and Manufacturing Processes***,** Vol. 15, No.. 1, pp. 97-105, 2000.

58. Cao, H. and M. WESSÉN, "Effect of Microstructure on Mechanical Properties of As-Cast Mg-Al Alloys", *Metallurgical and Materials Transactions A*, Vol. 35, No. 1 , pp. 309-319, 2000.

59. Konfidan, İ., *A New Approach to Magnesium Alloys for Powertrain Applications*, MSc. Thesis, Boğaziçi University, 2008.